

Ergodic Capacity Maximization of RIS-assisted Millimeter-Wave MIMO-OFDM Communication Systems

Renwang Li, Shu Sun, Meixia Tao, *Fellow, IEEE*

Abstract

Reconfigurable intelligent surface (RIS) has attracted extensive attentions in recent years. However, most research focuses on the scenario of the narrowband and/or instantaneous channel state information (CSI), while wide bandwidth with the use of millimeter-wave (mmWave) (including sub-THz) spectrum is a major trend in next-generation wireless communications, and statistical CSI is more practical to obtain in realistic systems. Thus, we fill the blank by looking at the ergodic capacity of RIS-assisted mmWave multiple-input multiple-output (MIMO) orthogonal frequency division multiplexing (OFDM) communication systems. The widely used Saleh-Valenzuela channel model is adopted to characterize the mmWave channels and only the statistical CSI is available. We first derive the approximations of the ergodic capacity by means of the majorization theory and Jensen's inequality. Then, an alternating optimization based algorithm is proposed to maximize the ergodic capacity by jointly designing the transmit covariance matrix at the base station and the reflection coefficients at the RIS. Specifically, the design of the transmit covariance matrix is transformed into a power allocation problem and solved by spatial-frequency water-filling. The reflection coefficients are optimized by the Riemannian conjugate gradient algorithm. Simulation results corroborate the closeness of the derived ergodic capacity approximations and the effectiveness of the proposed algorithms.

Index Terms

Reconfigurable intelligent surface, ergodic capacity, statistical channel state information (CSI), orthogonal frequency division multiplexing (OFDM), transmit covariance matrix, reflection coefficients.

R. Li, S. Sun, and M. Tao are with Department of Electronic Engineering, Shanghai Jiao Tong University, Shanghai, China (emails: {renwanglee, shusun, mxtao}@sjtu.edu.cn).

I. INTRODUCTION

The millimeter wave (mmWave) communication over the 30-300 GHz spectrum is one of the most promising techniques for 5G-and-beyond systems [1], [2]. However, the free-space path loss is more severe at mmWave compared to the conventional microwave bands. Typically, multiple-input multiple-output (MIMO) technology is employed to provide high beam gains to extend the transmission distance, but the high directivity makes the mmWave communication more sensitive to signal blockage. Meanwhile, MIMO technology greatly increases the consumption of power and cost. Recently, one promising and cost-effective solution to overcome these issues is to deploy Reconfigurable Intelligent Surface (RIS) [3]–[5]. An RIS is an artificial uniform planar array with plenty of elements, each of which can independently impose a phase shift on the incident signal and then reflect or refract it passively with the help of a smart controller. Hence, by adaptively adjusting the coefficients, RIS can be controlled to enhance the transmission quality of the desired signals. RIS is spectrum- and energy- efficient since it does not require radio frequency components. In addition, RIS can be flexibly and widely deployed so as to enhance the coverage of the mmWave communication.

Motivated by the above promising advantages, RIS has attracted extensive attentions from academia, e.g., [6]–[9]. The authors in [6] consider a power minimization problem under multiple-input single-output (MISO) scenario and propose a semidefinite relaxation (SDR) based algorithm to jointly optimize the active and passive beamforming, while the weighted sum-rate maximization problem is studied in [7]. The authors in [8] focus on the capacity maximization problem under MIMO scenario and propose an alternating optimization (AO) based algorithm. In [9], the inherent sparse feature of the mmWave channels is exploited to find an efficient algorithm to jointly design the transceiver and RIS.

However, all of the above works mainly focus on the narrowband communication systems, while 5G and future 6G communications are likely to conduct wideband deployment. Two main effects, i.e., spatial-wideband effect and frequency-wideband effect, emerge in mmWave MIMO wideband systems, which will dramatically affect the system performance [10], [11]. The spatial-wideband effect refers to the phenomenon of a non-negligible time delay across the array aperture for the same symbol in wideband systems. To combat the spatial-wideband effect, orthogonal frequency division multiplexing (OFDM) is a promising technology that divides the baseband

into several sub-bands so that each sub-band can be considered frequency-independent [10], [11]. As for the frequency-wideband effect which is also known as beam squint effect, there are no effective solutions thus far to the authors' best knowledge, especially for RIS. Specifically, the array response vectors differ across frequencies, notably for large bandwidth systems. However, RIS can only impose the same phase shifts on different frequencies since it is applied in the time domain and is lack of the ability of digital signal processing [12]. Consequently, there are a paucity of related works that investigate the wideband RIS-assisted communication systems [12]–[21]. For the single-input single-output (SISO) scenario, the authors in [12] aim at the achievable rate maximization and propose a successive convex approximation (SCA) based method for jointly power allocation and reflection coefficient optimization, while the problem of maximizing the minimum rate of all users is considered in [13]. For the MISO scenario, the authors in [14] focus on mitigating the beam squint effect and propose low-complexity solutions for both line-of-sight (LoS) and non-LoS scenarios. Multi-user MISO scenario is studied in [15], where the original sum rate maximization problem is reformulated as a modified mean square error (MSE) minimization problem, followed by a block coordinate descent (BCD) iterative algorithm. For the MIMO scenario, the authors in [16] aim at maximizing the spectral efficiency for point-to-point communication, while hybrid digital and analog beamforming is considered in [17], [18]. The weighted sum-rate maximization problem is studied in [19], where single data stream transmission is considered and the fractional programming is adopted to decouple the original problem. In addition, the secrecy rate maximization problem is investigated in [20] and an AO-based inexact block coordinate descent algorithm by leveraging Lagrange multiplier and complex circle manifold methods is proposed, while the discrete reflecting phase shift case is extended in [21].

However, all of the above contributions are based on the instantaneous channel state information (CSI), which is pretty challenging to acquire in practice since RIS is usually nearly passive and composed of a large number of unit cells [3]–[5]. An attractive alternative is to explore the statistical CSI. Therefore, we concentrate on a point-to-point RIS-assisted mmWave MIMO-OFDM communication system by exploiting the statistical CSI where the RIS is adopted as a reflecting surface. The main contributions of this study are summarized as follows:

- We focus on maximizing the ergodic capacity of the RIS-assisted mmWave MIMO-OFDM communication system. The widely used Saleh-Valenzuela (SV) channel model is adopted

to characterize the mmWave channels and only the statistical CSI is available. To the best of the authors' knowledge, this is the first effort to consider the statistical CSI in the broadband RIS-assisted mmWave MIMO-OFDM communication systems.

- We derive closed-form ergodic capacity approximations as well as an upper bound in the high signal-to-noise ratio (SNR) regime by means of the majorization theory and Jensen's inequality. The results show that the ergodic capacity increases logarithmically with the SNR, the number of the antennas at the base station (BS) and the user, the number of the reflecting units at the RIS, the power allocation at the BS, and the eigenvalues of the steering matrices associated with the BS, RIS and user.
- The ergodic capacity is maximized by jointly designing the transmit covariance matrix at the BS and the reflection coefficients at the RIS. Specifically, the design of the transmit covariance matrix is transformed into a power allocation problem and solved by spatial-frequency water-filling. The reflection coefficients are optimized by the Riemannian conjugate gradient (RCG) algorithm.

Furthermore, we conduct extensive simulations and validate the closeness of the derived ergodic capacity approximations as well as the upper bound. It is shown that our proposed alternating optimization algorithm outperforms the benchmark scheme from the literature [9]. In addition, the ergodic capacity after optimization can be improved by about 25 bps/Hz, which emphasizes the importance of the optimization of the transmit covariance matrix at the BS and the reflection coefficients at the RIS.

Finally, this work is a substantial improvement from our previous work [22]. On the one hand, this work takes the direct BS-user link into consideration, while it is assumed to be blocked due to unfavorable propagation conditions in [22]. When there exists the direct link, the majorization theory can not be applied directly because the cross product term of the ergodic capacity is no longer a positive semidefinite Hermitian matrix. Fortunately, the asymptotic orthogonality of the array response vectors can be utilized to overcome this difficulty. On the other hand, this work extends the narrowband scenario in [22] into the broadband systems. The spatial- and frequency-wideband effects are mitigated in our proposed algorithm.

The rest of the paper is organized as follows. Section II presents the system model and the problem formulation. The ergodic capacity approximations as well as the upper bound in high-SNR regime are derived in Section III. An alternating optimization algorithm for maximizing the

ergodic capacity is proposed in Section IV. The comparison with the state-of-the-art algorithms is discussed in Section V. Simulation results are provided in Section VI. Conclusions are drawn in Section VII.

Notations: The imaginary unit is denoted by $j = \sqrt{-1}$. Vectors and matrices are denoted by bold-face lower-case and upper-case letters, respectively. The conjugate, transpose and conjugate transpose of the vector \mathbf{x} are denoted by \mathbf{x}^* , \mathbf{x}^T and \mathbf{x}^H , respectively. The \odot symbol is the element-wise product and $\mathbb{E}(\cdot)$ is the expectation operation. The $\text{tr}(\cdot)$, $\text{det}(\cdot)$ and $\text{rank}(\cdot)$ denote the trace, determinant and rank operation, respectively. The $\Re\{\cdot\}$ operation extracts the real value of a complex variable. The $\text{unt}(\mathbf{x})$ operation represents an N -dimensional vector with elements $\frac{x_1}{|x_1|}, \dots, \frac{x_N}{|x_N|}$. The distribution of a circularly symmetric complex Gaussian random vector with mean vector μ and covariance matrix Σ is denoted by $\mathcal{CN}(\mu, \Sigma)$; and \sim stands for “distributed as”. The exponential random variable X with parameter λ is given by $X \sim \exp(\lambda)$.

II. SYSTEM MODEL AND PROBLEM FORMULATION

In this section, we will first introduce the RIS-assisted system model, then describe the widely adopted mmWave channel model, and finally propose the considered problem of maximizing the ergodic capacity.

A. System Model

We consider a downlink wideband point-to-point mmWave MIMO communication system as illustrated in Fig. 1, where the BS is equipped with N_b antennas and transmits signals to a user with N_u antennas, via the help of one N_r -element RIS. In order to mitigate the spatial-wideband effect of the wideband mmWave channel, OFDM with K subcarriers is employed to modulate the signal at the BS [10], [11]. Let $\mathbf{s}_k \in \mathbb{C}^{N_b \times 1}$ denote the transmitted signal vector at subcarrier k . The transmit covariance matrix at subcarrier k is defined as $\mathbf{Q}_k \triangleq \mathbb{E}\{\mathbf{s}_k \mathbf{s}_k^H\} \in \mathbb{C}^{N_b \times N_b}$, with $\mathbf{Q}_k \succeq \mathbf{0}$. The normalized transmit power constraint at the BS is given by

$$\sum_{k=1}^K \text{tr} \mathbb{E}\{\mathbf{s}_k \mathbf{s}_k^H\} = \sum_{k=1}^K \text{tr}(\mathbf{Q}_k) \leq 1. \quad (1)$$

Without loss of generality, we assume the maximum delay spread is of L_{\max} taps in the time domain for the baseband equivalent channels of both the BS-RIS-user reflecting link and the BS-user direct link. The transmit signal \mathbf{s}_k is first transformed into the time domain through a

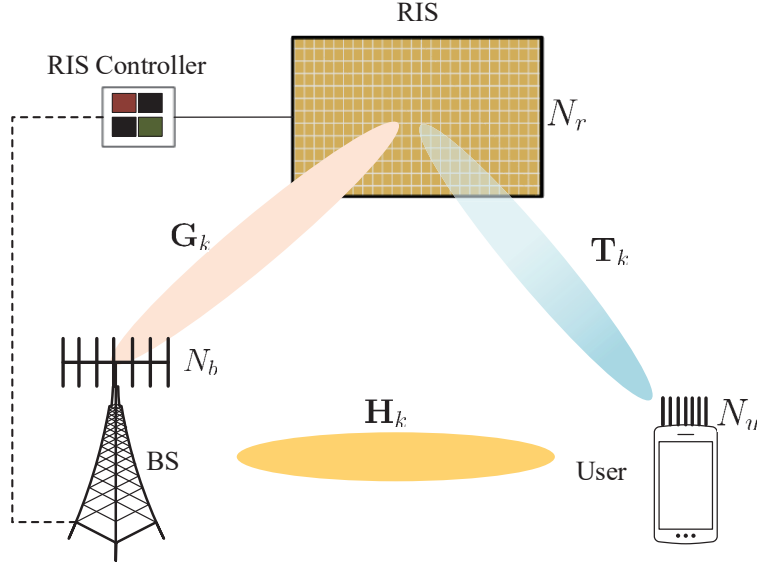


Fig. 1: Illustration of an RIS-aided mmWave MIMO-OFDM system.

K -point inverse discrete Fourier transform (IDFT), followed by the appending of a cyclic prefix (CP) of length N_{CP} , with $N_{\text{CP}} \geq L_{\text{max}}$. At the user side, after removing the CP and performing the K -point discrete Fourier transform (DFT), the baseband received signal $\mathbf{y}_k \in \mathbb{C}^{N_u \times 1}$ at the k -th subcarrier can be presented as

$$\mathbf{y}_k = (\mathbf{T}_k \mathbf{\Theta} \mathbf{G}_k + \mathbf{H}_k) \mathbf{s}_k + \mathbf{n}_k, \quad (2)$$

where $\mathbf{T}_k \in \mathbb{C}^{N_u \times N_r}$, $\mathbf{G}_k \in \mathbb{C}^{N_r \times N_b}$, and $\mathbf{H}_k \in \mathbb{C}^{N_u \times N_b}$ denote the frequency-domain channel on subcarrier k from the RIS to the user, from the BS to the RIS, and from the BS to the user, respectively; $\mathbf{\Theta} \in \mathbb{C}^{N_r \times N_r}$ denotes the response matrix at the RIS, which is written as

$$\mathbf{\Theta} \triangleq \text{diag}\{\xi_1 e^{j\theta_1}, \xi_2 e^{j\theta_2}, \dots, \xi_{N_r} e^{j\theta_{N_r}}\}, \quad (3)$$

where $\theta_i \in [0, 2\pi)$ and $\xi_i \in [0, 1]$ represent the phase shift and the amplitude reflection coefficient of the i -th reflecting unit, respectively; and $\mathbf{n}_k \sim \mathcal{CN}(\mathbf{0}, \sigma^2 \mathbf{I}_{N_u})$ represents the additive white Gaussian noise vector with zero mean and variance σ^2 ¹. Note that the RIS can only bring the same phase shift on different subcarriers due to the lack of the ability of digital signal processing [12]. In addition, the amplitude $\xi_i, \forall i \in \mathcal{N}_r$ is assumed to be one to maximize the

¹Without loss of generality, the variances of noise at different subcarriers are assumed to be the same.

signal reflection. Let $\mathcal{K} = \{1, \dots, K\}$ and $\mathcal{N}_r = \{1, \dots, N_r\}$ denote the index sets of subcarriers and RIS elements, respectively.

B. Channel Model

Due to the limited scattering paths in mmWave, the SV model is widely adopted for modelling the wideband mmWave channel. Suppose uniform linear arrays (ULAs) are equipped at the BS and the user, and a uniform planar array (UPA) is equipped at the RIS. The frequency domain channel matrix \mathbf{H}_k , \mathbf{G}_k and \mathbf{T}_k at subcarrier k can be expressed as [10], [11], [23]–[25]

$$\mathbf{H}_k = \sqrt{\frac{N_b N_u}{L_h}} \sum_{i=1}^{L_h} \alpha_{h,i} e^{-j2\pi\tau_{h,i} f_k} \mathbf{a}_r(\psi_{h,u,i}, f_k) \mathbf{a}_t^H(\psi_{h,b,i}, f_k), \quad (4)$$

$$\mathbf{G}_k = \sqrt{\frac{N_r N_b}{L_g}} \sum_{i=1}^{L_g} \alpha_{g,i} e^{-j2\pi\tau_{g,i} f_k} \mathbf{a}_r(\phi_{g,r,i}, \varphi_{g,r,i}, f_k) \mathbf{a}_t^H(\psi_{g,b,i}, f_k), \quad (5)$$

$$\mathbf{T}_k = \sqrt{\frac{N_r N_u}{L_t}} \sum_{i=1}^{L_t} \alpha_{t,i} e^{-j2\pi\tau_{t,i} f_k} \mathbf{a}_r(\psi_{t,u,i}, f_k) \mathbf{a}_t^H(\phi_{t,r,i}, \varphi_{t,r,i}, f_k), \quad (6)$$

where L_h (L_g, L_t) is the number of the paths between the BS and the user (the BS and the RIS, the RIS and the user); $\alpha_{h,i} \sim \mathcal{CN}(0, \sigma_{h,i}^2)$ ($\alpha_{g,i} \sim \mathcal{CN}(0, \sigma_{g,i}^2)$, $\alpha_{t,i} \sim \mathcal{CN}(0, \sigma_{t,i}^2)$)² denotes the complex gain of the i -th path and assume $\sigma_{h,1}^2 \geq \sigma_{h,2}^2 \geq \dots \geq \alpha_{h,L_h}^2$ ($\sigma_{g,1}^2 \geq \sigma_{g,2}^2 \geq \dots \geq \alpha_{g,L_g}^2$, $\sigma_{t,1}^2 \geq \sigma_{t,2}^2 \geq \dots \geq \alpha_{t,L_t}^2$); $\tau_{h,i}$ ($\tau_{g,i}, \tau_{t,i}$) is the delay of the i -th path; f_k is the frequency at subcarrier k , which is given by

$$f_k = f_c + \frac{f_s}{K} \left(k - 1 - \frac{K-1}{2} \right), \forall k \in \mathcal{K}, \quad (7)$$

where f_c is the carrier frequency and f_s is the bandwidth. Note that in the narrowband communication systems, it is assumed that $f_k = f_c$. However, this assumption is invalid in wideband communication systems and will dramatically affect the ergodic capacity. $\mathbf{a}_r(\cdot)$ ($\mathbf{a}_t(\cdot)$) denotes the normalized array response vector at the receiver side (the transmitter side); $\psi_{h,u,i}$ ($\psi_{t,u,i}$) denotes the angle of arrival (AoA) associated with the user of the direct link (the reflecting link); $\psi_{h,b,i}$ ($\psi_{g,b,i}$) denotes the angle of departure (AoD) associated with the BS of the direct link (the reflecting link); $\phi_{g,r,i}$ ($\phi_{t,r,i}$) and $\varphi_{g,r,i}$ ($\varphi_{t,r,i}$) denote the azimuth and elevation angles

²In mmWave MIMO communication systems, the complex gain is widely assumed to be i.i.d. random variables following the complex Gaussian distribution [23], [26].

of the arrival (departure) associated with the RIS. For a ULA with N antennas at the frequency f_k , the normalized array response vector is given by

$$\mathbf{a}(\psi, f_k) = \frac{1}{\sqrt{N}} \left[1, e^{j\frac{2\pi f_k d}{c} \sin \psi}, \dots, e^{j\frac{2\pi f_k d}{c} (N-1) \sin \psi} \right]^T, \quad (8)$$

where c represents the speed of light, $d = \frac{c}{2f_c} = \frac{\lambda}{2}$ is the antenna spacing, λ represents the signal wavelength of the central frequency, and ψ denotes the AoA or AoD. For a UPA with $M = M_y \times M_z$ elements at the frequency f_k , the normalized array response vector can be expressed as

$$\mathbf{a}(\phi, \varphi, f_k) = \frac{1}{\sqrt{M}} \left[1, \dots, e^{j\frac{2\pi f_k d_r}{c} (m_y \sin \phi \sin \varphi + m_z \cos \varphi)}, \dots, e^{j\frac{2\pi f_k d_r}{c} ((M_y-1) \sin \phi \sin \varphi + (M_z-1) \cos \varphi)} \right]^T, \quad (9)$$

where d_r is the unit cell spacing which is assumed to be half wavelength, ϕ and φ denote the azimuth and elevation angles, respectively. Defining $\mathbf{A}_{uh,k} = [\mathbf{a}_r(\psi_{h,u,1}, f_k), \dots, \mathbf{a}_r(\psi_{h,u,L_h}, f_k)] \in \mathbb{C}^{N_u \times L_h}$, $\mathbf{A}_{bh,k} = [\mathbf{a}_t(\psi_{h,b,1}, f_k), \mathbf{a}_t(\psi_{h,b,2}, f_k), \dots, \mathbf{a}_t(\psi_{h,b,L_h}, f_k)] \in \mathbb{C}^{N_b \times L_h}$, and $\mathbf{H}_{L,k} = \sqrt{\frac{N_u N_b}{L_h}} \text{diag}(\alpha_{h,1} e^{-j2\pi\tau_{h,1} f_k}, \alpha_{h,2} e^{-j2\pi\tau_{h,2} f_k}, \dots, \alpha_{h,L_h} e^{-j2\pi\tau_{h,L_h} f_k})$, the channel matrix \mathbf{H}_k in (4) can be rewritten as

$$\mathbf{H}_k = \mathbf{A}_{uh,k} \mathbf{H}_{L,k} \mathbf{A}_{bh,k}^H. \quad (10)$$

Defining $\mathbf{A}_{rg,k} = [\mathbf{a}_r(\phi_{g,r,1}, \varphi_{g,r,1}, f_k), \mathbf{a}_r(\phi_{g,r,2}, \varphi_{g,r,2}, f_k), \dots, \mathbf{a}_r(\phi_{g,r,L_g}, \varphi_{g,r,L_g}, f_k)] \in \mathbb{C}^{N_r \times L_g}$, $\mathbf{A}_{bg,k} = [\mathbf{a}_t(\psi_{g,b,1}, f_k), \dots, \mathbf{a}_t(\psi_{g,b,L_g}, f_k)] \in \mathbb{C}^{N_b \times L_g}$, and $\mathbf{G}_{L,k} = \sqrt{\frac{N_r N_b}{L_g}} \text{diag}(\alpha_{g,1} e^{-j2\pi\tau_{g,1} f_k}, \alpha_{g,2} e^{-j2\pi\tau_{g,2} f_k}, \dots, \alpha_{g,L_g} e^{-j2\pi\tau_{g,L_g} f_k})$, the channel matrix \mathbf{G}_k in (5) can be expressed as

$$\mathbf{G}_k = \mathbf{A}_{rg,k} \mathbf{G}_{L,k} \mathbf{A}_{bg,k}^H. \quad (11)$$

Defining $\mathbf{A}_{rt,k} = [\mathbf{a}_t(\phi_{t,r,1}, \varphi_{t,r,1}, f_k), \mathbf{a}_t(\phi_{t,r,2}, \varphi_{t,r,2}, f_k), \dots, \mathbf{a}_t(\phi_{t,r,L_t}, \varphi_{t,r,L_t}, f_k)] \in \mathbb{C}^{N_r \times L_t}$, $\mathbf{A}_{ut,k} = [\mathbf{a}_r(\psi_{t,u,1}, f_k), \dots, \mathbf{a}_r(\psi_{t,u,L_t}, f_k)] \in \mathbb{C}^{N_u \times L_t}$, and $\mathbf{T}_{L,k} = \sqrt{\frac{N_r N_u}{L_t}} \text{diag}(\alpha_{t,1} e^{-j2\pi\tau_{t,1} f_k}, \alpha_{t,2} e^{-j2\pi\tau_{t,2} f_k}, \dots, \alpha_{t,L_t} e^{-j2\pi\tau_{t,L_t} f_k})$, the channel matrix \mathbf{T}_k in (6) can be presented as

$$\mathbf{T}_k = \mathbf{A}_{ut,k} \mathbf{T}_{L,k} \mathbf{A}_{rt,k}^H. \quad (12)$$

C. Problem Formulation

Assume the instantaneous CSI is unknown, the ergodic capacity of the RIS-assisted mmWave MIMO-OFDM communication system is given by

$$C(\{\mathbf{Q}_k\}_{k=1}^K, \Theta) = \max_{\sum_{k=1}^K \text{Tr}(\mathbf{Q}_k) \leq 1} \mathbb{E}_{\mathbf{H}_{\text{eff}}} \left[\frac{1}{K + N_{\text{cp}}} \sum_{k=1}^K \log_2 \det \left(\mathbf{I}_{N_u} + \frac{P_T}{\sigma^2} \mathbf{H}_{\text{eff},k} \mathbf{Q}_k \mathbf{H}_{\text{eff},k}^H \right) \right], \quad (13)$$

where $P_T > 0$ is the power budget at the BS, and $\mathbf{H}_{\text{eff},k} = \mathbf{T}_k \Theta \mathbf{G}_k + \mathbf{H}_k$ denotes the effective channel at subcarrier k between the BS and the user. In this paper, we aim to maximize the ergodic capacity by jointly designing the transmit covariance matrix $\{\mathbf{Q}_k\}_{k=1}^K$ at the BS and the reflection coefficients Θ at the RIS, subject to the maximum power budget at the BS. Therefore, the optimization problem can be formulated as

$$\mathcal{P}_0 : \max_{\{\mathbf{Q}_k\}_{k=1}^K, \Theta} C(\{\mathbf{Q}_k\}_{k=1}^K, \Theta) \quad (14a)$$

$$\text{s.t.} \quad \sum_{k=1}^K \text{tr}(\mathbf{Q}_k) \leq 1, \quad (14b)$$

$$\mathbf{Q}_k \succeq 0, \forall k \in \mathcal{K}, \quad (14c)$$

$$\Theta = \text{diag}(e^{j\theta_1}, e^{j\theta_2}, \dots, e^{j\theta_{N_r}}). \quad (14d)$$

The problem \mathcal{P}_0 is highly challenging mainly due to the following three facts. First of all, there is no explicit expression of the ergodic capacity and the expectation operation in (13) prevents further optimization. Secondly, the problem is non-convex due to the unit-modulus constraints of the RIS, and thus difficult to be optimally solved. Last but not the least, different from the narrowband communication systems, the RIS can only apply the same phase shifts over different subcarriers. Thereby, we need to consider all of the subcarriers when designing the RIS. In the following, we will firstly find an explicit expression to approximate the ergodic capacity, and then maximize the ergodic capacity by jointly designing $\{\mathbf{Q}_k\}_{k=1}^K$ and Θ .

III. ERGODIC CAPACITY APPROXIMATIONS

In this section, the approximations as well as the high-SNR upper bound of the ergodic capacity are firstly derived by means of the majorization theory. The Jensen's inequality is then used to obtain explicit and compact expressions.

A. Approximations of the Ergodic Capacity

The derivation of the ergodic capacity is much more difficult than that in our previous work [22], where the direct link is blocked by obstacles. In the previous work, [27, Theorem 9.H.1.a] is frequently adopted during the derivation. However, when the direct BS-user link exists, the cross product term $\mathbf{H}_k \mathbf{Q}_k \mathbf{G}_k^H \Theta^H \mathbf{T}_k^H$ of the ergodic capacity is not a positive semi-definite Hermitian matrix, which prevents further derivation. Fortunately, we have the following proposition.

Proposition 1: When N_b goes to infinity, we have

$$\mathbf{G}_k \mathbf{H}_k^H \rightarrow \mathbf{0}^{N_r \times N_u}. \quad (15)$$

Proof: The AoDs of different scattering paths can be considered as continuous random variables that are independent from each other. Then, the event $E = \{\phi_{b,i} \neq \varphi_{b,j}, \forall i \in \{1, 2, \dots, L_g\}, \forall j \in \{1, 2, \dots, L_h\}\}$ occurs with probability one. Therefore, by the asymptotic orthogonality of ULA array response vectors [9], [28], we have

$$\mathbf{A}_{bg,k}^H \mathbf{A}_{bh,k} \rightarrow \mathbf{0}^{L_g \times L_h}, \quad \text{as } N_b \rightarrow \infty. \quad (16)$$

Consequently, $\mathbf{G}_k \mathbf{H}_k^H = \mathbf{A}_{rg,k} \mathbf{G}_{L,k} \mathbf{A}_{bg,k}^H \mathbf{A}_{bh,k} \mathbf{H}_{L,k}^H \mathbf{A}_{uh,k}^H \rightarrow \mathbf{0}^{N_r \times N_u}$. ■

Proposition 1 implies that the cross product term of the ergodic capacity can be neglected, when there does not exist the transmit covariance matrix \mathbf{Q}_k and the number of the antennas at the BS is sufficiently large. Under **Proposition 1** and the majorization theory [27], several approximations of the ergodic capacity are derived, which are presented in the following theorems.

Theorem 1: Under the wideband SV channel model expressed in (10), (11) and (12), when the number of antennas at the BS goes to infinity, the ergodic capacity of the RIS-assisted mmWave MIMO-OFDM communication systems can be approximated by

$$\begin{aligned} C_{app} = & \mathbb{E}_{\alpha_{g,i}, \alpha_{t,i}} \left[\frac{1}{K + N_{cp}} \sum_{k=1}^K \sum_{i=1}^{N_{s1}} \log_2 \left(1 + \frac{P_T}{\sigma^2} \frac{N_b N_u N_r^2}{L_g L_t} q_{k,i} d_{ut,k,i} d_{bg,k,i} d_{r,k,i} |\alpha_{g,i}|^2 |\alpha_{t,i}|^2 \right) \right] \\ & + \mathbb{E}_{\alpha_{h,i}} \left[\frac{1}{K + N_{cp}} \sum_{k=1}^K \sum_{i=1}^{N_{s2}} \log_2 \left(1 + \frac{P_T}{\sigma^2} \frac{N_b N_u}{L_h} q_{k, N_{s1}+i} d_{uh,k,i} d_{bh,k,i} |\alpha_{h,i}|^2 \right) \right], \end{aligned} \quad (17)$$

where $N_{s1} = \min(\text{rank}(\mathbf{A}_{bg,k}^H \mathbf{A}_{bg,k}), \text{rank}(\mathbf{A}_{ut,k}^H \mathbf{A}_{ut,k}), \text{rank}(\mathbf{X}_{r,k}^H \mathbf{X}_{r,k}))$ denotes the rank of the BS-RIS-user reflecting link, $\mathbf{X}_{r,k} = \mathbf{A}_{rt,k}^H \mathbf{\Theta} \mathbf{A}_{rg,k}$; $N_{s2} = \min(\text{rank}(\mathbf{A}_{bh,k}^H \mathbf{A}_{bh,k}), \text{rank}(\mathbf{A}_{uh,k}^H \mathbf{A}_{uh,k}))$ denotes the rank of the BS-user direct link; $q_{k,i}$ is the power allocated to the i -th data stream, \mathbf{Q}_k is determined by (46); $(d_{ut,k,1}, d_{ut,k,2}, \dots, d_{ut,k,N_{s1}})$, $(d_{bg,k,1}, d_{bg,k,2}, \dots, d_{bg,k,N_{s1}})$, $(d_{r,k,1}, d_{r,k,2}, \dots, d_{r,k,N_{s1}})$, $(d_{uh,k,1}, d_{uh,k,2}, \dots, d_{uh,k,N_{s1}})$ and $(d_{bh,k,1}, d_{bh,k,2}, \dots, d_{bh,k,N_{s1}})$ are descending ordered eigenvalues of $\mathbf{A}_{ut,k}^H \mathbf{A}_{ut,k}$, $\mathbf{A}_{bg,k}^H \mathbf{A}_{bg,k}$, $\mathbf{X}_{r,k}^H \mathbf{X}_{r,k}$, $\mathbf{A}_{uh,k}^H \mathbf{A}_{uh,k}$ and $\mathbf{A}_{bh,k}^H \mathbf{A}_{bh,k}$, respectively.

Proof: See Appendix A. ■

It is found that the ergodic capacity is closely related to the eigenvalues of the matrices associated with the BS, the user and the RIS, i.e., $\mathbf{A}_{ut,k}^H \mathbf{A}_{ut,k}$, $\mathbf{A}_{bg,k}^H \mathbf{A}_{bg,k}$, $\mathbf{X}_{r,k}^H \mathbf{X}_{r,k}$, $\mathbf{A}_{uh,k}^H \mathbf{A}_{uh,k}$

and $\mathbf{A}_{bh,k}^H \mathbf{A}_{bh,k}$. The RIS-assisted mmWave MIMO communication systems are likely to operate in the high-SNR regime by virtue of beamforming techniques with large antenna arrays. Thus, an upper bound in the high-SNR regime is obtained in the following theorem.

Theorem 2: Under the wideband SV channel model expressed in (10), (11) and (12), when the number of antennas at the BS goes to infinity, the ergodic capacity of the RIS-assisted mmWave MIMO-OFDM communication systems in the high-SNR regime can be upper bounded by

$$C_h^{upper} = \sum_{k=1}^K \sum_{i=1}^{N_{s1}} \frac{1}{(K + N_{cp}) \ln 2} \left(-2\gamma + \ln \left(\frac{P_T N_b N_u N_r^2 \sigma_{g,i}^2 \sigma_{t,i}^2}{\sigma^2 L_g L_t} q_{k,i} d_{ut,k,i} d_{bg,k,i} d_{r,k,i} \right) \right) \\ + \sum_{k=1}^K \sum_{i=1}^{N_{s2}} \frac{1}{(K + N_{cp}) \ln 2} \left(-\gamma + \ln \left(\frac{P_T N_b N_u \sigma_{h,i}^2}{\sigma^2 L_h} q_{k,N_{s1}+i} d_{uh,k,i} d_{bh,k,i} \right) \right), \quad (18)$$

where C_h^{upper} refers to the upper bound in the high-SNR regime; $\gamma \approx 0.5772$ refers to the Euler-Mascheroni constant; N_{s1} , N_{s2} , $q_{k,i}$, $d_{ut,k,i}$, $d_{bg,k,i}$, $d_{r,k,i}$, $d_{uh,k,i}$ and $d_{bh,k,i}$ are defined the same as in **Theorem 1**.

Proof: See Appendix B. ■

It can be found that when the SNR is large, the upper bound of the ergodic capacity increases logarithmically with SNR, N_b , N_u , N_r , the power allocation $q_{k,i}$, and the eigenvalues of the matrices $\mathbf{A}_{ut,k}^H \mathbf{A}_{ut,k}$, $\mathbf{A}_{bg,k}^H \mathbf{A}_{bg,k}$, $\mathbf{X}_{r,k}^H \mathbf{X}_{r,k}$, $\mathbf{A}_{uh,k}^H \mathbf{A}_{uh,k}$ and $\mathbf{A}_{bh,k}^H \mathbf{A}_{bh,k}$.

B. Jensen's Approximations for the Ergodic Capacity

The expectation operation in (17) hinders further optimization. To overcome this difficulty, Jensen's inequality is adopted to obtain simplified expressions.

Theorem 3: Under the wideband SV channel model expressed in (10), (11) and (12), when the number of antennas at the BS goes to infinity, the ergodic capacity of the RIS-assisted mmWave MIMO-OFDM communication systems can be approximated by

$$C_{Jen1} = \frac{1}{K + N_{cp}} \sum_{k=1}^K \sum_{i=1}^{N_{s1}} \log_2 \left(1 + \frac{P_T N_b N_u N_r^2 \sigma_{g,i}^2 \sigma_{t,i}^2}{\sigma^2 L_g L_t} q_{k,i} d_{ut,k,i} d_{bg,k,i} d_{r,k,i} \right) \\ + \frac{1}{K + N_{cp}} \sum_{k=1}^K \sum_{i=1}^{N_{s2}} \log_2 \left(1 + \frac{P_T N_b N_u \sigma_{h,i}^2}{\sigma^2 L_h} q_{k,N_{s1}+i} d_{uh,k,i} d_{bh,k,i} \right). \quad (19)$$

Proof: See Appendix C. ■

It is worth noting that the above approximation C_{Jen1} has a very compact form composed of the product of the eigenvalues and the summation over data streams. The ergodic capacity

approximation consists of two parts, i.e., the BS-RIS-user reflection part and the BS-user direct part. The reflection part is determined by SNR, the number of antennas of the BS and the user, the number of the reflection units of the RIS, the power allocation at the BS, and the eigenvalues of the matrices of $\mathbf{A}_{ut,k}^H \mathbf{A}_{ut,k}$, $\mathbf{A}_{bh,k}^H \mathbf{A}_{bh,k}$ and $\mathbf{X}_{r,k}^H \mathbf{X}_{r,k}$. The direct part is influenced by SNR, the number of antennas of the BS and the user, the power allocation at the BS, and the eigenvalues of the matrices of $\mathbf{A}_{uh,k}^H \mathbf{A}_{uh,k}$ and $\mathbf{A}_{bh,k}^H \mathbf{A}_{bh,k}$. Similar to previous works [22] and [29], the approximation C_{Jen1} is loose, and we can find a tighter approximation by means of order statistic [30]. Specifically, we have the following theorem.

Theorem 4: Under the wideband SV channel model expressed in (10), (11) and (12), when the number of antennas at the BS goes to infinity, the ergodic capacity of the RIS-assisted mmWave MIMO-OFDM communication systems can be approximated by

$$C_{Jen2} = \frac{1}{K + N_{cp}} \sum_{k=1}^K \left[\sum_{i=1}^{N_{s2}} \log_2 \left(1 + \sum_{j=1}^i \frac{1}{L_h - j + 1} \frac{P_T N_b N_u \sigma_{h,i}^2}{\sigma^2 L_h} q_{k, N_{s1} + i} d_{uh,k,i} d_{bh,k,i} \right) + \sum_{i=1}^{N_{s1}} \log_2 \left(1 + \sum_{j=1}^i \frac{1}{L_g - j + 1} \sum_{j=1}^i \frac{1}{L_t - j + 1} \frac{P_T N_b N_u N_r^2 \sigma_{g,i}^2 \sigma_{t,i}^2}{L_g L_t} q_{k,i} d_{ut,k,i} d_{bg,k,i} d_{r,k,i} \right) \right]. \quad (20)$$

Proof: The proof is similar to [22, Proposition 4] and [29, Proposition 3]. Thus, it is omitted owing to space limitations. ■

Note that the approximation C_{Jen2} exhibits a tighter approximation than C_{Jen1} since the Jensen's upper bound is minimized by the order statistic. Therefore, the approximation C_{Jen2} in (20) is adopted in the following optimization.

In addition, when no CSI is available at the BS, uniform power allocation over transmit signals, i.e., $\mathbf{Q}_k = \frac{1}{KN_b} \mathbf{I}_{N_b}$, is optimal [31]. In this case, we have the following proposition.

Proposition 2: Under the wideband SV channel model expressed in (10), (11) and (12), when the number of antennas at the BS goes to infinity and $\mathbf{Q}_k = \frac{1}{KN_b} \mathbf{I}_{N_b}$, the upper bound of the ergodic capacity in the high-SNR regime is given by

$$C_h^{upper} = \sum_{k=1}^K \sum_{i=1}^{N_{s1}} \frac{1}{(K + N_{cp}) \ln 2} \left(-2\gamma + \ln \left(\frac{P_T N_u N_r^2 \sigma_{g,i}^2 \sigma_{t,i}^2}{\sigma^2 K L_g L_t} d_{ut,k,i} d_{bg,k,i} d_{r,k,i} \right) \right) + \sum_{k=1}^K \sum_{i=1}^{N_{s2}} \frac{1}{(K + N_{cp}) \ln 2} \left(-\gamma + \ln \left(\frac{P_T N_u \sigma_{h,i}^2}{\sigma^2 K L_h} d_{uh,k,i} d_{bh,k,i} \right) \right), \quad (21)$$

The Jensen's approximation can be expressed as

$$\begin{aligned}
C_{Jen1} &= \frac{1}{K + N_{cp}} \sum_{k=1}^K \left[\sum_{i=1}^{N_{s1}} \log_2 \left(1 + \frac{P_T N_u N_r^2 \sigma_{g,i}^2 \sigma_{t,i}^2}{\sigma^2 K L_g L_t} d_{ut,k,i} d_{bg,k,i} d_{r,k,i} \right) \right. \\
&\quad \left. + \sum_{i=1}^{N_{s2}} \log_2 \left(1 + \frac{P_T N_u \sigma_{h,i}^2}{\sigma^2 K L_h} d_{uh,k,i} d_{bh,k,i} \right) \right] \\
C_{Jen2} &= \frac{1}{K + N_{cp}} \sum_{k=1}^K \left[\sum_{i=1}^{N_{s2}} \log_2 \left(1 + \sum_{j=1}^i \frac{1}{L_h - j + 1} \frac{P_T N_u \sigma_{h,i}^2}{\sigma^2 K L_h} d_{uh,k,i} d_{bh,k,i} \right) \right. \\
&\quad \left. + \sum_{i=1}^{N_{s1}} \log_2 \left(1 + \sum_{j=1}^i \frac{1}{L_g - j + 1} \sum_{j=1}^i \frac{1}{L_t - j + 1} \frac{P_T N_u N_r^2 \sigma_{g,i}^2 \sigma_{t,i}^2}{\sigma^2 K L_g L_t} d_{ut,k,i} d_{bg,k,i} d_{r,k,i} \right) \right] \tag{22}
\end{aligned}$$

Proof: See Appendix D. ■

It is worth noting that the ergodic capacity approximations are derived for an arbitrary positive semidefinite Hermitian matrix \mathbf{Q} in our previous work [22]. However, in this work, the ergodic capacity approximations can be derived only when \mathbf{Q}_k satisfies (46) or $\mathbf{Q}_k = \frac{1}{KN_b} \mathbf{I}_{N_b}$ due to the existence of the BS-user direct link.

IV. TRANSMIT COVARIANCE MATRIX AND REFLECTION COEFFICIENTS OPTIMIZATION

With the obtained approximation expression C_{Jen2} of the ergodic capacity of the RIS-assisted mmWave MIMO-OFDM communication systems, we now concentrate on maximizing the ergodic capacity by jointly designing the transmit covariance matrix $\{\mathbf{Q}_k\}_{k=1}^K$ and the reflection coefficients Θ . Note that \mathbf{Q}_k is determined by (46). Thus, we only need to optimize $q_{k,i}$, instead of \mathbf{Q}_k . Applying C_{Jen2} in (20) to the problem \mathcal{P}_0 , we have

$$\mathcal{P}_1 : \max_{q_{k,i}, \Theta} C_{Jen2} \tag{23a}$$

$$\text{s.t.} \quad \sum_{k=1}^K \sum_{i=1}^{N_s} q_{k,i} \leq 1, \tag{23b}$$

$$q_{k,i} \geq 0, \forall i, k, \tag{23c}$$

$$\Theta = \text{diag} (e^{j\theta_1}, e^{j\theta_2}, \dots, e^{j\theta_{N_r}}), \tag{23d}$$

where

$$C_{Jen2} = \frac{1}{K + N_{cp}} \sum_{k=1}^K \left[\sum_{i=1}^{N_{s2}} \log_2 \left(1 + \sum_{j=1}^i \frac{1}{L_h - j + 1} \frac{P_T N_b N_u \sigma_{h,i}^2}{\sigma^2} q_{k,N_{s1}+i} d_{uh,k,i} d_{bh,k,i} \right) + \sum_{i=1}^{N_{s1}} \log_2 \left(1 + \sum_{j=1}^i \frac{1}{L_g - j + 1} \sum_{j=1}^i \frac{1}{L_t - j + 1} \frac{P_T N_b N_u N_r^2 \sigma_{g,i}^2 \sigma_{t,i}^2}{L_g L_t} q_{k,i} d_{ut,k,i} d_{bg,k,i} d_{r,k,i} \right) \right]. \quad (24)$$

Compared with problem \mathcal{P}_0 , problem \mathcal{P}_1 is much simpler, where the objective function is only composed of the summation of simple logarithm functions. However, the problem \mathcal{P}_1 is still challenging mainly due to two facts. First of all, the problem \mathcal{P}_1 is not jointly convex over $q_{k,i}$ and Θ . Thus, the optimal solution is very difficult to obtain. Secondly, the reflection coefficients Θ are not directly related to the objective function. We need to build the bridge to connect Θ and the objective function. In the following, AO is adopted to decouple the problem \mathcal{P}_1 into two sub-problems, and then different tools are employed to optimize them.

A. Transmit Covariance Matrix Optimization

Since \mathbf{Q}_k is determined by (46), the problem of optimizing transmit covariance matrix can be transformed into a power allocation problem. Specifically, when the reflection coefficients Θ is fixed, the problem \mathcal{P}_1 is simplified as following,

$$\max_{q_{k,i}} \quad \frac{1}{K + N_{cp}} \sum_{k=1}^K \sum_{i=1}^{N_s} \log_2 (1 + \zeta_{k,i} q_{k,i}) \quad (25a)$$

$$\text{s.t.} \quad \sum_{k=1}^K \sum_{i=1}^{N_s} q_{k,i} \leq 1, \quad (25b)$$

$$q_{k,i} \geq 0, \forall i, k, \quad (25c)$$

where

$$\zeta_{k,i} = \begin{cases} \sum_{j=1}^i \frac{1}{L_g - j + 1} \sum_{j=1}^i \frac{1}{L_t - j + 1} \frac{P_T N_b N_u N_r^2 \sigma_{g,i}^2 \sigma_{t,i}^2}{L_g L_t} d_{ut,k,i} d_{bg,k,i} d_{r,k,i}, & \text{if } 1 \leq i \leq N_{s1}, \\ \sum_{j=1}^i \frac{1}{L_h - j + 1} \frac{P_T N_b N_u \sigma_{h,i}^2}{\sigma^2} d_{uh,k,i} d_{bh,k,i}, & \text{if } N_{s1} + 1 \leq i \leq N_s. \end{cases} \quad (26)$$

The above problem is well studied in [32]. It is found that joint space-frequency water-filling outperforms single dimensional water-filling either in the spatial domain or in the frequency domain. The optimal power allocation $q_{k,i}$ across subcarriers and streams is given by

$$q_{k,i} = \max \left(0, \frac{1}{q_0} - \frac{1}{\zeta_{k,i}} \right), \quad (27)$$

where q_0 is the water level satisfying $\sum_{k=1}^K \sum_{i=1}^{N_s} q_{k,i} = 1$.

B. Reflection Coefficient Optimization

When the power allocations $q_{k,i}$ are fixed, the problem \mathcal{P}_1 can be rewritten as (with constant terms ignored)

$$\min_{\Theta} \quad - \sum_{k=1}^K \sum_{i=1}^{N_{s1}} \log_2(1 + \eta_{k,i} d_{r,k,i}) \quad (28a)$$

$$\text{s.t.} \quad \Theta = \text{diag}(e^{j\theta_1}, e^{j\theta_2}, \dots, e^{j\theta_{N_r}}), \quad (28b)$$

where $\eta_{k,i} = \sum_{j=1}^i \frac{1}{L_g - j + 1} \sum_{j=1}^i \frac{1}{L_t - j + 1} \frac{P_T}{\sigma^2} \frac{N_b N_u N_r^2 \sigma_g^2 \sigma_{t,i}^2}{L_g L_t} q_{k,i} d_{ut,k,i} d_{bg,k,i}$. For better understanding, the information of $d_{r,k,i}$ is rewritten down here: $d_{r,k,i}$ are the descending ordered eigenvalues of $\mathbf{X}_{r,k}^H \mathbf{X}_{r,k}$, where $\mathbf{X}_{r,k} = \mathbf{A}_{rt,k}^H \Theta \mathbf{A}_{rg,k}$, $\mathbf{X}_{r,k}^H \mathbf{X}_{r,k} = \mathbf{U}_{r,k} \mathbf{D}_{r,k} \mathbf{U}_{r,k}^H$, $\mathbf{D}_{r,k} = \text{diag}(d_{r,k,1}, d_{r,k,2}, \dots, d_{r,k,L_g})$. The above problem is highly challenging due to the following two facts. On the one hand, problem (28) is non-convex due to the unit-modulus constraints, and thus difficult to solve optimally. On the other hand, the objective function is connected to the optimization variable via eigenvalue decomposition (EVD) rather than being directly tied to it. A sub-optimal solution of Θ can be obtained using the RCG algorithm which is widely applied in RIS-aided systems [7], [9]. Define $\boldsymbol{\theta} = [e^{j\theta_1}, e^{j\theta_2}, \dots, e^{j\theta_{N_r}}]^T \in \mathbb{C}^{N_r \times 1}$ and $f(\boldsymbol{\theta}) = - \sum_{k=1}^K \sum_{i=1}^{N_{s1}} \log_2(1 + \eta_{k,i} d_{r,k,i})$. Then, the feasible set of $\boldsymbol{\theta}$ forms a Riemannian manifold $\mathcal{M} = \{\boldsymbol{\theta} \in \mathbb{C}^{N_r \times 1} : |\theta_i| = 1, \forall i\}$ [33]. The RCG algorithm usually has three key steps in each iteration.

1) *Riemannian Gradient*: The Riemannian gradient $\text{grad} f(\boldsymbol{\theta})$ is the orthogonal projection of the Euclidean gradient $\nabla f(\boldsymbol{\theta})$ onto the manifold:

$$\text{grad} f(\boldsymbol{\theta}) = \nabla f(\boldsymbol{\theta}) - \Re\{\nabla f(\boldsymbol{\theta}) \odot \boldsymbol{\theta}^*\} \odot \boldsymbol{\theta}. \quad (29)$$

In the following, we will explore the Euclidean gradient of $f(\boldsymbol{\theta})$.

For simplicity, let us first consider subcarrier k . Specifically, following the chain rule, the ℓ -th element of the gradient is given by

$$\left(\frac{\partial f(\boldsymbol{\theta})}{\partial \bar{\theta}_\ell^H} \right)_k = \left[\frac{\partial d_{r,k,1}}{\partial \bar{\theta}_\ell^H} \quad \frac{\partial d_{r,k,2}}{\partial \bar{\theta}_\ell^H} \quad \dots \quad \frac{\partial d_{r,k,N_{s1}}}{\partial \bar{\theta}_\ell^H} \right] \begin{bmatrix} \frac{\partial f(\boldsymbol{\theta})}{\partial d_{r,k,1}} \\ \frac{\partial f(\boldsymbol{\theta})}{\partial d_{r,k,2}} \\ \vdots \\ \frac{\partial f(\boldsymbol{\theta})}{\partial d_{r,k,N_{s1}}} \end{bmatrix}, \quad (30)$$

where $\bar{\theta}_\ell$ denotes the ℓ -th element of $\boldsymbol{\theta}$, $\left(\frac{\partial f(\boldsymbol{\theta})}{\partial \bar{\theta}_\ell^H}\right)_k$ denotes the ℓ -th element of the gradient on subcarrier k , and the overall gradient can be represented as

$$\begin{aligned}\nabla f(\boldsymbol{\theta}) &= \left[\frac{\partial f(\boldsymbol{\theta})}{\partial \bar{\theta}_1^H}, \frac{\partial f(\boldsymbol{\theta})}{\partial \bar{\theta}_2^H}, \dots, \frac{\partial f(\boldsymbol{\theta})}{\partial \bar{\theta}_{N_r}^H} \right]^T \\ &= \left[\sum_{k=1}^K \left(\frac{\partial f(\boldsymbol{\theta})}{\partial \bar{\theta}_1^H} \right)_k, \sum_{k=1}^K \left(\frac{\partial f(\boldsymbol{\theta})}{\partial \bar{\theta}_2^H} \right)_k, \dots, \sum_{k=1}^K \left(\frac{\partial f(\boldsymbol{\theta})}{\partial \bar{\theta}_{N_r}^H} \right)_k \right]^T.\end{aligned}\quad (31)$$

The partial derivative of $f(\boldsymbol{\theta})$ with respect to $d_{r,k,i}$ can be found by directly differentiating $f(\boldsymbol{\theta})$ to be

$$\frac{\partial f(\boldsymbol{\theta})}{\partial d_{r,k,i}} = -\frac{\eta_{k,i}}{(1 + \eta_{k,i} d_{r,k,i}) \ln 2} \quad (32)$$

Then, we will explore the partial derivative of $d_{r,k,i}$ with respect to the ℓ -th reflection coefficient.

First of all, $d_{r,k,i}$ can be expressed as

$$\begin{aligned}d_{r,k,i} &= \mathbf{u}_{k,i}^H \mathbf{X}_{r,k}^H \mathbf{X}_{r,k} \mathbf{u}_{k,i} \\ &= \mathbf{u}_{k,i}^H \mathbf{A}_{rg,k}^H \boldsymbol{\Theta}^H \mathbf{A}_{rt,k} \mathbf{A}_{rt,k}^H \boldsymbol{\Theta} \mathbf{A}_{rg,k} \mathbf{u}_{k,i},\end{aligned}\quad (33)$$

where $\mathbf{u}_{k,i}$ refers to the i -th column of $\mathbf{U}_{r,k}$. Then, the partial derivative with respect to $\bar{\theta}_\ell^H$ can be calculated as

$$\begin{aligned}\frac{\partial d_{r,k,i}}{\partial \bar{\theta}_\ell^H} &= \frac{\partial \mathbf{u}_{k,i}^H}{\partial \bar{\theta}_\ell^H} \mathbf{X}_{r,k}^H \mathbf{X}_{r,k} \mathbf{u}_{k,i} + \mathbf{u}_{k,i}^H \frac{\partial (\mathbf{X}_{r,k}^H \mathbf{X}_{r,k})}{\partial \bar{\theta}_\ell^H} \mathbf{u}_{k,i} + \mathbf{u}_{k,i}^H \mathbf{X}_{r,k}^H \mathbf{X}_{r,k} \frac{\partial \mathbf{u}_{k,i}}{\partial \bar{\theta}_\ell^H} \\ &\stackrel{(a)}{=} d_{r,k,i} \frac{\partial \mathbf{u}_{k,i}^H}{\partial \bar{\theta}_\ell^H} \mathbf{u}_{k,i} + \mathbf{u}_{k,i}^H \frac{\partial (\mathbf{X}_{r,k}^H \mathbf{X}_{r,k})}{\partial \bar{\theta}_\ell^H} \mathbf{u}_{k,i} + d_{r,k,i} \mathbf{u}_{k,i}^H \frac{\partial \mathbf{u}_{k,i}}{\partial \bar{\theta}_\ell^H} \\ &\stackrel{(b)}{=} \mathbf{u}_{k,i}^H \frac{\partial (\mathbf{X}_{r,k}^H \mathbf{X}_{r,k})}{\partial \bar{\theta}_\ell^H} \mathbf{u}_{k,i} \\ &= \mathbf{u}_{k,i}^H \frac{\partial (\mathbf{A}_{rg,k}^H \boldsymbol{\Theta}^H \mathbf{A}_{rt,k} \mathbf{A}_{rt,k}^H \boldsymbol{\Theta} \mathbf{A}_{rg,k})}{\partial \bar{\theta}_\ell^H} \mathbf{u}_{k,i},\end{aligned}\quad (34)$$

where (a) holds due to the fact that $\mathbf{X}_{r,k}^H \mathbf{X}_{r,k} \mathbf{u}_{k,i} = d_{r,k,i} \mathbf{u}_{k,i}$ and $\mathbf{u}_{k,i}^H \mathbf{X}_{r,k}^H \mathbf{X}_{r,k} = d_{r,k,i} \mathbf{u}_{k,i}^H$ by the definition of eigenvalues, and (b) follows $\mathbf{u}_{k,i}^H \mathbf{u}_{k,i} = 1$.

The (x, y) -th entry of $\mathbf{X}_{r,k}^H \mathbf{X}_{r,k}$ can be represented as

$$[\mathbf{X}_{r,k}^H \mathbf{X}_{r,k}]_{x,y} = \sum_{m=1}^{N_r} \sum_{n=1}^{N_r} [\mathbf{A}_{rg,k}^H]_{x,m} \bar{\theta}_m^H [\mathbf{A}_{rt,k} \mathbf{A}_{rt,k}^H]_{m,n} \bar{\theta}_n [\mathbf{A}_{rg,k}]_{n,y} \quad (35)$$

Algorithm 1 RCG Algorithm for Reflection Coefficients Optimization

- 1: **Input:** $\{\eta_{k,i}, \mathbf{A}_{rt,k}, \mathbf{A}_{rg,k}\}$, desired accuracy ϵ
 - 2: Initialize: $\boldsymbol{\theta}_0, \boldsymbol{\eta}_0 = -\text{grad } f(\boldsymbol{\theta}_0)$ and set $i = 0$;
 - 3: **repeat**
 - 4: Choose the Armijo backtracking line search step size α ;
 - 5: Update $\boldsymbol{\theta}$ by using (40);
 - 6: Update the Riemannian gradient by using (29);
 - 7: Update the research direction by using (38);
 - 8: $i \leftarrow i + 1$;
 - 9: **until** $\|\text{grad } f(\boldsymbol{\theta}_i)\|_2 \leq \epsilon$.
-

yielding the partial derivative with respect to $\bar{\theta}_\ell^H$

$$\left[\frac{\partial (\mathbf{X}_{r,k}^H \mathbf{X}_{r,k})}{\partial \bar{\theta}_\ell^H} \right]_{x,y} = \sum_{n=1, n \neq \ell}^{N_r} [\mathbf{A}_{rg,k}^H]_{x,\ell} [\mathbf{A}_{rt,k} \mathbf{A}_{rt,k}^H]_{\ell,n} \bar{\theta}_n [\mathbf{A}_{rg,k}]_{n,y} \quad (36)$$

Thus, the partial derivative of $\mathbf{X}_{r,k}^H \mathbf{X}_{r,k}$ with respect to $\bar{\theta}_\ell^H$ can be expressed as

$$\frac{\partial (\mathbf{X}_{r,k}^H \mathbf{X}_{r,k})}{\partial \bar{\theta}_\ell^H} = \sum_{n=1, n \neq \ell}^{N_r} [\mathbf{A}_{rg,k}^H]_{:, \ell} \otimes \left([\mathbf{A}_{rt,k} \mathbf{A}_{rt,k}^H]_{\ell, n} \bar{\theta}_n [\mathbf{A}_{rg,k}]_{n, :} \right), \quad (37)$$

where \otimes denotes the Kronecker product operation. Finally, by substituting (30), (32), (34) and (37) back into (31), we can obtain the gradient $f(\boldsymbol{\theta})$.

2) *Search Direction:* The current search direction $\boldsymbol{\eta}$ can be found as

$$\boldsymbol{\eta} = -\text{grad } f(\boldsymbol{\theta}) + \beta \mathcal{T}(\bar{\boldsymbol{\eta}}), \quad (38)$$

where β is chosen as the Polak-Ribiere parameter to achieve fast convergence [33], $\bar{\boldsymbol{\eta}}$ is the previous search direction, and $\mathcal{T}(\cdot)$ is a transport operation defined as

$$\mathcal{T}(\boldsymbol{\eta}) = \boldsymbol{\eta} - \Re\{\boldsymbol{\eta} \odot \boldsymbol{\theta}^*\} \odot \boldsymbol{\theta}. \quad (39)$$

3) *Retraction:* The retraction operation is to project the tangent vector back to the manifold:

$$\boldsymbol{\theta} \leftarrow \text{unt}(\boldsymbol{\theta} + \alpha \boldsymbol{\eta}), \quad (40)$$

where α is the Armijo backtracking line search step size [33].

Algorithm 2 Alternating Optimization Algorithm for Problem \mathcal{P}_1

- 1: Initialize: $q_{k,i}^{(0)} = \frac{1}{KN_s}$, $\Theta^{(0)}$ is randomly generated where the phases $\{\theta_\ell\}_{\forall \ell}$ are uniformly and independently distributed in $[0, 2\pi)$, error tolerance ϵ , and set $i = 0$;
 - 2: **repeat**
 - 3: Calculate $q_{k,i}^{(i+1)}$ according to (27) with fixed $\Theta^{(i)}$;
 - 4: Calculate $\Theta^{(i+1)}$ based on **Algorithm 1** with fixed $q_{k,i}^{(i+1)}$;
 - 5: $i \leftarrow i + 1$;
 - 6: **until** The increase of the objective value of the problem \mathcal{P}_1 is below the threshold ϵ .
-

The key steps are introduced above, and the consequent RCG algorithm for reflection coefficients optimization is summarized in **Algorithm 1**, which is guaranteed to converge to a stationary point [33].

V. SUMMARY AND DISCUSSIONS

In this section, we will first discuss the convergence and the complexity of the proposed algorithm, and then compare it with other state-of-the-art methods [8], [9]. It is worth noting that our proposed algorithm relies on the statistical CSI, while the algorithms in [8], [9] depend on the instantaneous CSI. Moreover, we only compare the computational complexity and performance in the single carrier scenario due to the following facts. Firstly, the authors in [8] alternately optimize N_r reflection coefficients and the transmit covariance matrix. In the single carrier scenario, the closed-form solution at each step is obtained. However, in the wideband scenario, CVX is needed at each step, which necessitates $N_r + 1$ times of CVX for one round, resulting in very high and unaffordable computational complexity, especially for a large number of reflecting units of RIS. The methods in [8] is more competitive in the single carrier scenario. Secondly, the methods in [9] are designed based on narrowband systems and can not be extended to wideband systems directly.

A. Converge and Computational Complexity Analysis

In summary, the proposed algorithm is illustrated in **Algorithm 2**. Let us first consider the convergence of the proposed algorithm. We adopt the AO framework in **Algorithm 2**. First of

Algorithm	Dominant computational complexity	Type of CSI
Proposed algorithm	$\mathcal{O}(I_1 I_2 N_{s_1} N_r^2 L_g^2 + (L_g^2 + L_h^2) N_b)$	statistical CSI
AO-based algorithm in [8]	$\mathcal{O}(2N_u^2 N_b N_r I)$	instantaneous CSI
T-SVD-BF in [9]	$\mathcal{O}(N_r L_1 + N_u^2 N_b)$	instantaneous CSI

TABLE I: Algorithm Comparison under Single Carrier Case.

all, the optimal power allocation is obtained via (27) with fixed reflection coefficients. Then, the sub-optimal reflection coefficients are obtained via **Algorithm 1** with fixed power allocation. Therefore, the objective value of the problem \mathcal{P}_1 is non-decreasing over iterations and the proposed algorithm is guaranteed to converge.

Next, let us consider the complexity of the proposed **Algorithm 2**. Firstly, the complexity of the water-filling algorithm is dominated by the procedure of singular value decomposition (SVD). Note that \mathbf{Q}_k is determined by (46), and optimizing \mathbf{Q}_k is transformed into power allocation in (27) whose complexity can be neglected. Secondly, the complexity of reflection coefficient optimization is dominated by the calculation of the gradient in (31). The complexity of calculating (34) is $\mathcal{O}(N_r L_g^2)$. The complexity of calculating (31) is $\mathcal{O}(K N_{s_1} N_r^2 L_g^2)$. And the complexity of calculating (46) is $\mathcal{O}(N_b(L_g^2 + L_h^2))$. Note that \mathbf{Q}_k in (46) only needs to be calculated once. Thus, the overall complexity of the proposed **Algorithm 2** is on the order of $\mathcal{O}(I_1 I_2 K N_{s_1} N_r^2 L_g^2 + K N_b(L_g^2 + L_h^2))$, where I_1 and I_2 denote the number of iterations of **Algorithm 1** and **Algorithm 2** required to converge, respectively.

B. Computational Complexity Comparison

In this subsection, we compare the computational complexity with other state-of-the-art methods [8], [9] under the single carrier scenario. Let us first consider the AO-based algorithm [8], which is designed for general channels. The complexity of AO-based algorithm [8] is on the order of $\mathcal{O}(N_u N_b (N_r + \min(N_u, N_b)) L + ((3N_u^3 + 2N_u^2 N_b + N_b^2) N_r + N_u N_b \min(N_u, N_b) I))$, where L denotes the number of realizations for initialization and I denotes the number of outer iterations [8]. The authors in [9] propose an algorithm called Truncated SVD based beamforming (T-SVD-BF) specifically for mmWave systems which utilizes the inherent sparse structure of mmWave channels. The complexity of T-SVD-BF [9] is on the order of $\mathcal{O}(N_r L_1 + N_b N_u \min(N_b, N_u))$, where L_1 denotes the number of iterations required to converge when optimizing the reflection

coefficients. Considering the case $N_b \geq N_u$, the dominant computational complexity of the respective algorithms is summarized in Table I. We can find that our proposed algorithm only requires statistical CSI with slightly higher computational complexity.

VI. SIMULATION RESULTS

In this part, we first investigate the closeness of the derived approximations of the ergodic capacity of RIS-assisted mmWave MIMO-OFDM communication systems, and then evaluate the performance of the proposed algorithm. Let us first consider the details of the channels as illustrated in Section II-B. The central carrier frequency is $f_c = 28$ GHz, the number of carriers is $K = 128$, and the bandwidth is $f_s = 1$ GHz. The angles $\psi_{h,b,i}$, $\psi_{g,b,i}$, $\psi_{h,u,i}$ and $\psi_{t,u,i}$ are randomly generated and uniformly distributed in $[-\pi, \pi)$, $\phi_{g,r,i}$ and $\phi_{t,r,i}$ in $[-\pi/2, \pi/2]$, and $\varphi_{g,r,i}$ and $\varphi_{t,r,i}$ in $[0, \pi]$. The exponential distribution is adopted to model the variances of the complex gain [34]. In order to make the complex gain of the direct link and the reflecting link comparable, we set $\sigma_{h,i}^2 \sim \exp(1)$, $\sigma_{g,i}^2 \sim \exp(0.1)$ and $\sigma_{t,i}^2 \sim \exp(0.1)$. Other system parameters are set as follows unless specified otherwise later: $N_{CP} = 32$, $N_b = 64$, $N_r = 10 \times 10$, $N_u = 16$, $L_h = 6$, $L_g = 6$, $L_t = 6$. In the first part, we set $q_{k,i} = \frac{1}{KN_s}$, \mathbf{Q}_k is determined by (46) and Θ is randomly generated where the phases $\{\theta_\ell\}_{\forall \ell}$ are uniformly and independently distributed in $[0, 2\pi)$. All simulation curves are averaged over 1000 independent channel realizations.

A. Closeness of the Derived Ergodic Capacity Approximations

Fig. 2 illustrates the ergodic capacity against the transmit SNR. For ease of understanding, we plot $\max(C_h^{upper}, 0)$ instead of C_h^{upper} . There are some interesting findings. First of all, in our previous work [22] where the direct link does not exist, the derived ergodic capacity approximation C_{Jen2} fits the Monte-Carlo results well. However, when the direct link exists, all of the approximations are larger than the Monte-Carlo results in the high-SNR region. It is mainly due to the following two facts. On the one hand, **Proposition 1** utilizes the asymptotic orthogonality of array response vectors. However, the number of antennas at the BS is usually limited in practice, which leads to $\mathbf{G}_k \mathbf{H}_k^H \neq \mathbf{0}^{N_r \times N_u}$. On the other hand, the optimal \mathbf{Q}_k is closely related to the end-to-end instantaneous channel $\mathbf{H}_{\text{eff},k}$, but only the statistical CSI is available. Thus, the adopted transmit covariance matrix \mathbf{Q}_k in (46) is sub-optimal, resulting in

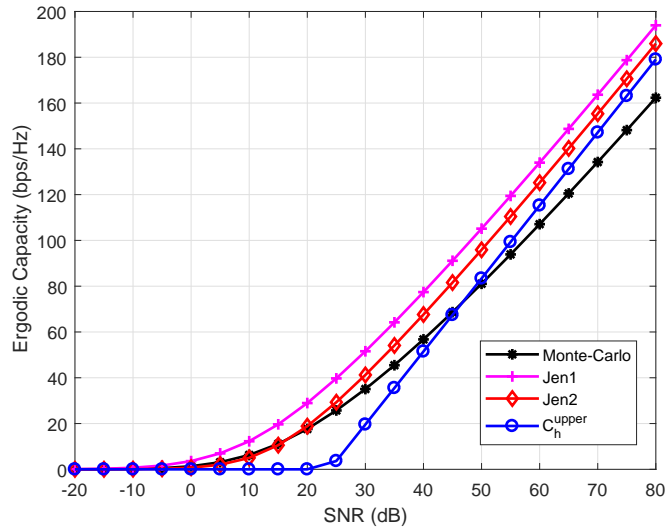


Fig. 2: Ergodic capacity against the transmit SNR.

some errors. Nevertheless, the trend of the derived approximations is consistent with the Monte-Carlo results. And it will be shown later that the proposed algorithm outperforms T-SVD-BF in [9]. Secondly, C_{Jen1} and C_{Jen2} are larger than the Monte-Carlo results because they are amplified by the Jensen's inequality. By means of order statistic, C_{Jen2} is more compatible with the Monte-Carlo results than C_{Jen1} . Therefore, it is reasonable to adopt C_{Jen2} to approximate the ergodic capacity in Section IV. Thirdly, the upper bound C_h^{upper} of the ergodic capacity is valid only when the transmit SNR is larger than about 45 dB, since it is devised specifically for high SNRs.

B. Performance of the Proposed Algorithms

Fig. 3 illustrates the convergence performance of the proposed **Algorithm 2** with SNR = 10 dB. It is found that the proposed algorithm converges within 10 iterations, which confirms the convergence of the proposed algorithm.

In Fig. 4, the proposed algorithm is compared with some benchmarks under single carrier scenario, where AO and T-SVD-BF refers to the method in [8] and [9], respectively, and “Not Optimized” denotes the scenario where $q_{k,i} = \frac{1}{KN_s}$ and Θ is randomly generated. It is interesting that our proposed algorithm performs well although the derived ergodic capacity approximation C_{Jen2} is larger than the Monte-Carlo results. On the one hand, the AO-based algorithm in [8] performs best since it finds the optimal solution in each iteration. However, the AO-based

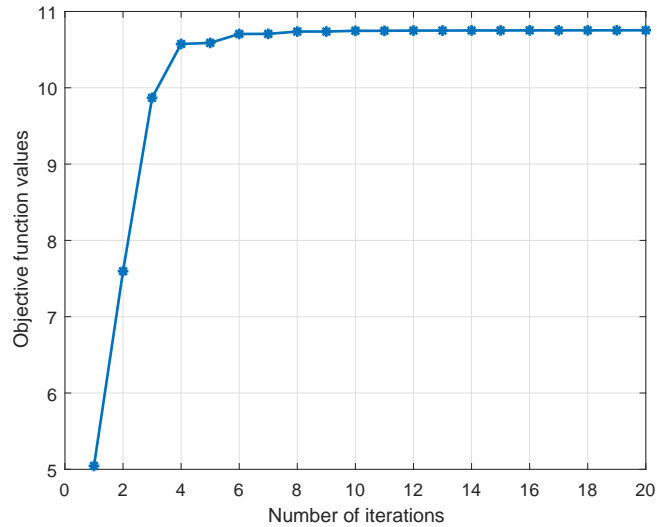


Fig. 3: Convergence of the proposed **Algorithm 2** with SNR = 10 dB.

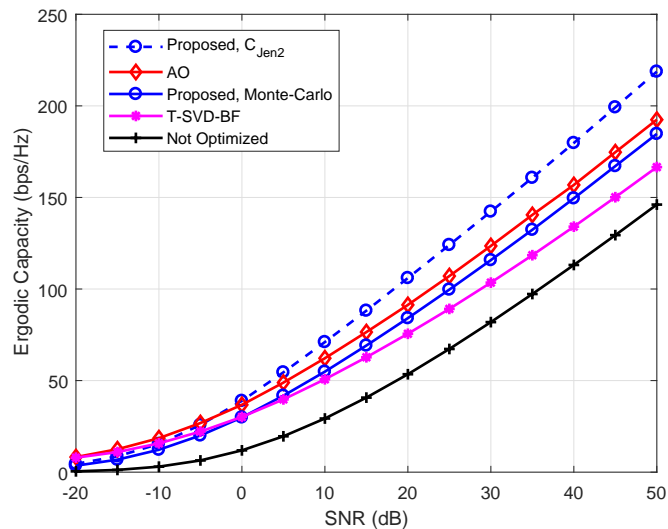


Fig. 4: Performance comparison with benchmarks under single carrier scenario.

algorithm needs to optimize each unit of RIS alternately which causes a pretty high computational time, especially for a large number of reflection units of RIS. The gap between our proposed algorithm and the AO-based algorithm is small, which is about 8 bps/Hz on average. On the other hand, the proposed algorithm outperforms T-SVD-BF when SNR is larger than 0 dB. Both T-SVD-BF and our proposed algorithm utilize the asymptotic orthogonality of array response vectors. The T-SVD-BF algorithm requires both BS and user sides to employ a large number of antennas to approximate the SVD of the reflecting channel. However, our proposed algorithm

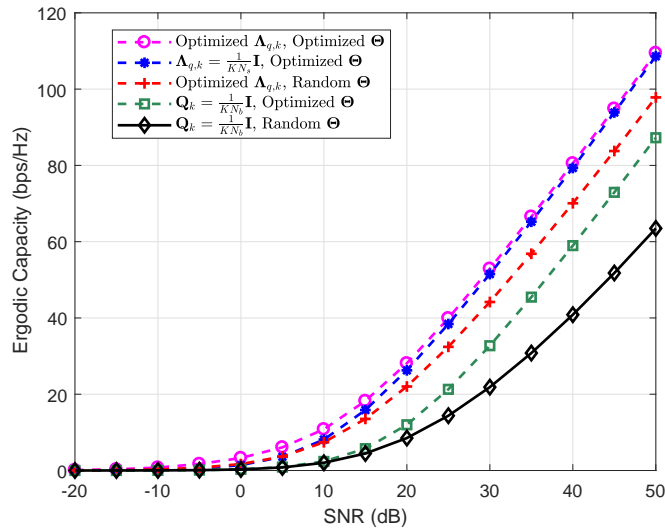


Fig. 5: Influence comparison between transmit covariance matrix and reflection coefficients, Jensen's approximation.

only requires the BS side to employ a large number of antennas. Nevertheless, the complexity of T-SVD-BF is the least and all the three algorithms improve the ergodic capacity greatly compared with the curve "Not Optimized". Note that our proposed algorithm only requires statistical CSI, while the AO-based algorithm and T-SVD-BF require instantaneous CSI. Overall, our proposed algorithm is quite favorable in practice considering the performance, computational complexity, and CSI feedback overhead.

We compare the influence on the ergodic capacity of the transmit covariance matrix and reflection coefficients in Fig. 5 and Fig. 6, where the dotted lines represent Jensen's approximation C_{Jen2} and the solid lines represent the corresponding Monte-Carlo results. When $\mathbf{Q}_k = \frac{1}{KN_b} \mathbf{I}$, the Jensen's approximation C_{Jen2} in (22) is adopted in the optimization. Let's focus on the Monte-Carlo results in Fig. 6 since these exclude approximation errors and are more suitable for fair comparison. We first find that the ergodic capacity of equal power allocation approaches that of the optimized power allocation, especially when the SNR is greater than 10 dB. Then, compared with the curve " $\mathbf{Q}_k = \frac{1}{KN_b} \mathbf{I}$, Random Θ ", the ergodic capacity can be improved by about 8 bps/Hz if only the reflection coefficients Θ are optimized when SNR is larger than 40 dB. The ergodic capacity can be improved by about 16 bps/Hz if only the transmit covariance matrix is optimized, while the ergodic capacity can be improved by about 25 bps/Hz if both the reflection coefficients and the transmit covariance matrix are optimized. These observations

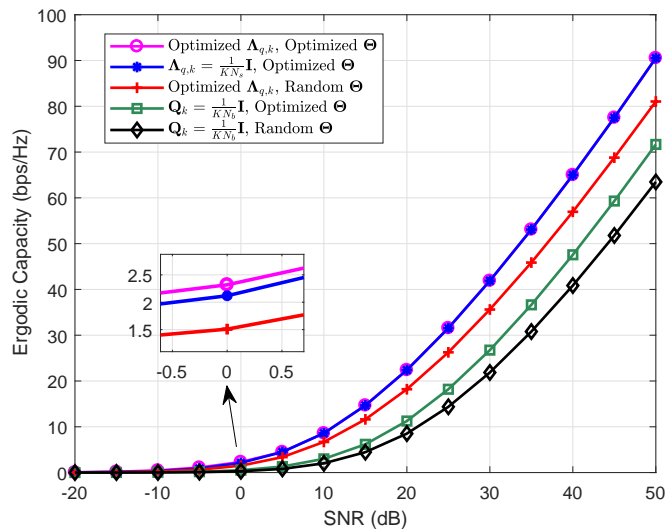


Fig. 6: Influence comparison between transmit covariance matrix and reflection coefficients, Monte-Carlo results.

indicate that the design of the reflection coefficients and the transmit covariance matrix plays a crucial role for ergodic capacity.

VII. CONCLUSION

This paper studies the ergodic capacity maximization problem for the point-to-point RIS-assisted mmWave MIMO-OFDM communication systems. First of all, the compact closed-form approximations of the ergodic capacity are derived by means of the majorization theory and Jensen's inequality. The approximations show that the ergodic capacity increases logarithmically with SNR, the number of antennas at the BS and the user, the number of the reflection units at the RIS, the power allocation at the BS, and the eigenvalues of the matrices associated with the BS, the user and the RIS. Then, an AO-based algorithm is proposed to maximize the ergodic capacity by jointly optimizing the transmit covariance matrix at the BS and the reflection coefficients at the RIS, where the transmit covariance matrix is optimized by spatial-frequency water-filling and the reflection coefficients are optimized by the RCG algorithm. Simulation results validate the closeness of the derived ergodic capacity approximations and the effectiveness of the proposed algorithms. The ergodic capacity after optimization can be improved by about 25 bps/Hz, which emphasizes the importance of the optimization of the transmit covariance matrix and the reflection coefficients.

APPENDIX

A. Proof of Theorem 1

Let us first focus on subcarrier k , and then extend the results to all of the subcarriers. Define the singular value decomposition (SVD) of $\mathbf{H}_{\text{eff},k}$ as $\mathbf{H}_{\text{eff},k} = \mathbf{U}\mathbf{\Sigma}\mathbf{V}^H$. If the instantaneous CSI $\mathbf{H}_{\text{eff},k}$ is known, the optimal transmit covariance matrix \mathbf{Q}_k is given by

$$\mathbf{Q}_k = \mathbf{V}_1 \mathbf{\Lambda}_k \mathbf{V}_1^H, \quad (41)$$

where \mathbf{V}_1 represents the first N_s columns of \mathbf{V} , N_s represents the rank of $\mathbf{H}_{\text{eff},k}$, $\mathbf{\Lambda}_k = \text{diag}(q_{k,1}, q_{k,2}, \dots, q_{k,N_s})$ where $q_{k,i}$ represents the optimal amount of power allocated to the i -th data stream. Then, we have

$$\begin{aligned} C_k &= \mathbb{E}_{\mathbf{H}_{\text{eff},k}} \left[\log_2 \det \left(\mathbf{I}_{N_u} + \frac{P_T}{\sigma^2} \mathbf{H}_{\text{eff},k} \mathbf{Q}_k \mathbf{H}_{\text{eff},k}^H \right) \right] \\ &= \mathbb{E}_{\mathbf{H}_{\text{eff},k}} \left[\sum_{i=1}^{N_s} \log_2 \left(1 + \frac{P_T}{\sigma^2} q_{k,i} |\mathbf{\Sigma}(i,i)|^2 \right) \right] \\ &= \mathbb{E}_{\mathbf{H}_{\text{eff},k}} \left[\sum_{i=1}^{N_s} \log_2 \left(1 + \frac{P_T}{\sigma^2} q_{k,i} \lambda_i (\mathbf{H}_{\text{eff},k} \mathbf{H}_{\text{eff},k}^H) \right) \right] \\ &\stackrel{(a)}{=} \mathbb{E}_{\mathbf{H}_{\text{eff},k}} \left[\sum_{i=1}^{N_s} \log_2 \left(1 + \frac{P_T}{\sigma^2} q_{k,i} \lambda_i (\mathbf{T}_k \mathbf{\Theta} \mathbf{G}_k \mathbf{G}_k^H \mathbf{\Theta}^H \mathbf{T}_k^H + \mathbf{H}_k \mathbf{H}_k^H) \right) \right] \\ &\stackrel{(b)}{=} \mathbb{E}_{\mathbf{H}_{\text{eff},k}} \left[\sum_{i=1}^{N_{s1}} \log_2 \left(1 + \frac{P_T}{\sigma^2} q_{k,i} \lambda_i (\mathbf{T}_k \mathbf{\Theta} \mathbf{G}_k \mathbf{G}_k^H \mathbf{\Theta}^H \mathbf{T}_k^H) \right) \right. \\ &\quad \left. + \sum_{i=1}^{N_{s2}} \log_2 \left(1 + \frac{P_T}{\sigma^2} q_{k,i+N_{s1}} \lambda_i (\mathbf{H}_k \mathbf{H}_k^H) \right) \right], \end{aligned} \quad (42)$$

where C_k refers to the ergodic capacity at subcarrier k , $\lambda_i(\cdot)$ refers to the i -th largest eigenvalue of the input matrix, (a) holds due to the **Proposition 1**, (b) holds due to the asymptotic orthogonality of \mathbf{G}_k and \mathbf{H}_k^H , N_{s1} is the rank of the BS-RIS-user cascade channel, N_{s2} is the rank of the direct BS-user channel, and it follows that $N_s = N_{s1} + N_{s2}$.

Define $\mathbf{X}_{r,k} = \mathbf{A}_{rt,k}^H \mathbf{\Theta} \mathbf{A}_{rg,k}$, and assume the eigenvalue decompositions (EVD) of $\mathbf{A}_{ut,k}^H \mathbf{A}_{ut,k}$, $\mathbf{A}_{bg,k}^H \mathbf{A}_{bg,k}$, $\mathbf{X}_{r,k}^H \mathbf{X}_{r,k}$, $\mathbf{A}_{uh,k}^H \mathbf{A}_{uh,k}$ and $\mathbf{A}_{bh,k}^H \mathbf{A}_{bh,k}$ can be expressed as follows,

$$\begin{aligned} \mathbf{A}_{ut,k}^H \mathbf{A}_{ut,k} &= \mathbf{U}_{ut,k}^H \mathbf{D}_{ut,k} \mathbf{U}_{ut,k}, \\ \mathbf{A}_{bg,k}^H \mathbf{A}_{bg,k} &= \mathbf{U}_{bg,k}^H \mathbf{D}_{bg,k} \mathbf{U}_{bg,k}, \end{aligned}$$

$$\begin{aligned}
\mathbf{X}_{r,k}^H \mathbf{X}_{r,k} &= \mathbf{U}_{r,k}^H \mathbf{D}_{r,k} \mathbf{U}_{r,k}, \\
\mathbf{A}_{uh,k}^H \mathbf{A}_{uh,k} &= \mathbf{U}_{uh,k}^H \mathbf{D}_{uh,k} \mathbf{U}_{uh,k}, \\
\mathbf{A}_{bh,k}^H \mathbf{A}_{bh,k} &= \mathbf{U}_{bh,k}^H \mathbf{D}_{bh,k} \mathbf{U}_{bh,k},
\end{aligned} \tag{43}$$

where $\mathbf{U}_{ut,k}$, $\mathbf{U}_{bg,k}$, $\mathbf{U}_{r,k}$, $\mathbf{U}_{uh,k}$, and $\mathbf{U}_{bh,k}$ are the eigenvectors of $\mathbf{A}_{ut,k}^H \mathbf{A}_{ut,k}$, $\mathbf{A}_{bg,k}^H \mathbf{A}_{bg,k}$, $\mathbf{X}_{r,k}^H \mathbf{X}_{r,k}$, $\mathbf{A}_{uh,k}^H \mathbf{A}_{uh,k}$ and $\mathbf{A}_{bh,k}^H \mathbf{A}_{bh,k}$, respectively; $\mathbf{D}_{ut,k} = \text{diag}(d_{ut,k,1}, d_{ut,k,2}, \dots, d_{ut,k,L_t})$, $\mathbf{D}_{bg,k} = \text{diag}(d_{bg,k,1}, d_{bg,k,2}, \dots, d_{bg,k,L_g})$, $\mathbf{D}_{r,k} = \text{diag}(d_{r,k,1}, d_{r,k,2}, \dots, d_{r,k,L_r})$, $\mathbf{D}_{uh,k} = \text{diag}(d_{uh,k,1}, d_{uh,k,2}, \dots, d_{uh,k,L_h})$, $\mathbf{D}_{bh,k} = \text{diag}(d_{bh,k,1}, d_{bh,k,2}, \dots, d_{bh,k,L_b})$, and $d_{ut,k,i}$, $d_{bg,k,i}$, $d_{r,k,i}$, $d_{uh,k,i}$, $d_{bh,k,i} \geq 0$ are the eigenvalue of $\mathbf{A}_{ut,k}^H \mathbf{A}_{ut,k}$, $\mathbf{A}_{bg,k}^H \mathbf{A}_{bg,k}$, $\mathbf{X}_{r,k}^H \mathbf{X}_{r,k}$, $\mathbf{A}_{uh,k}^H \mathbf{A}_{uh,k}$ and $\mathbf{A}_{bh,k}^H \mathbf{A}_{bh,k}$ in descending order, respectively.

Using the results in [22, Theorem 1] and [29, Theorem 1], we have

$$\begin{aligned}
C_{app,k} &= \mathbb{E}_\lambda \left[\log_2 \det \left(\mathbf{I}_{N_{s2}} + \frac{P_T}{\sigma^2} \mathbf{\Lambda}_k^2 \odot \boldsymbol{\lambda}(\mathbf{A}_{uh,k}^H \mathbf{A}_{uh,k}) \odot \boldsymbol{\lambda}(\mathbf{A}_{bh,k}^H \mathbf{A}_{bh,k}) \odot \boldsymbol{\lambda}(\mathbf{H}_{L,k}^H \mathbf{H}_{L,k}) \right) \right] \\
&\quad + \mathbb{E}_\lambda \left[\log_2 \det \left(\mathbf{I}_{N_{s1}} + \frac{P_T}{\sigma^2} \mathbf{\Lambda}_k^1 \odot \boldsymbol{\lambda}(\mathbf{A}_{ut,k}^H \mathbf{A}_{ut,k}) \odot \boldsymbol{\lambda}(\mathbf{A}_{bg,k}^H \mathbf{A}_{bg,k}) \odot \boldsymbol{\lambda}(\mathbf{X}_{r,k}^H \mathbf{X}_{r,k}) \right) \right] \\
&\quad \odot \boldsymbol{\lambda}(\mathbf{T}_{L,k}^H \mathbf{T}_{L,k}) \odot \boldsymbol{\lambda}(\mathbf{G}_{L,k}^H \mathbf{G}_{L,k}) \Big] \\
&= \mathbb{E}_{\alpha_{g,i}, \alpha_{t,i}} \left[\sum_{i=1}^{N_{s1}} \log_2 \left(1 + \frac{P_T}{\sigma^2} \frac{N_b N_u N_r^2}{L_g L_t} q_{k,i} d_{ut,k,i} d_{bg,k,i} d_{r,k,i} |\alpha_{g,i}|^2 |\alpha_{t,i}|^2 \right) \right] \\
&\quad + \mathbb{E}_{\alpha_{h,i}} \left[\sum_{i=1}^{N_{s2}} \log_2 \left(1 + \frac{P_T}{\sigma^2} \frac{N_b N_u}{L_h} q_{k,N_{s1}+i} d_{uh,k,i} d_{bh,k,i} |\alpha_{h,i}|^2 \right) \right]
\end{aligned} \tag{44}$$

where $C_{app,k}$ denotes the approximation of C_k , $\mathbf{\Lambda}_k^1 = \text{diag}(q_{1,k}, q_{2,k}, \dots, q_{N_{s1},k})$, $\mathbf{\Lambda}_k^2 = \text{diag}(q_{N_{s1}+1}, q_{N_{s1}+2}, \dots, q_{N_s})$ and $\boldsymbol{\lambda}(\mathbf{Y}) = [\lambda_1(\mathbf{Y}), \lambda_2(\mathbf{Y}), \dots, \lambda_n(\mathbf{Y})]^T$.

Note that the above results are based on the knowledge of the instantaneous CSI of $\mathbf{H}_{\text{eff},k}$. However, only the statistical CSI is available in many practical systems and hence the assumption in this work. Meanwhile, we find that the optimization of the transmit covariance matrix is strongly related to the steering matrix at the BS. Physically, when there are L different paths, the BS can transmit at most L data streams. Then, we can firstly align the transmit covariance matrix towards these paths and allocate different power over them later. Therefore, one reasonable and sub-optimal design of the transmit covariance matrix \mathbf{Q}_k is to determine its directions according

to $\mathbf{A}_{bg,k}$ and $\mathbf{A}_{bh,k}$. Specifically, define the SVD of $\mathbf{A}_{bg,k}$ and $\mathbf{A}_{bh,k}$ as

$$\begin{aligned}\mathbf{A}_{bg,k} &= \mathbf{U}_2 \boldsymbol{\Sigma}_2 \mathbf{V}_2^H, \\ \mathbf{A}_{bh,k} &= \mathbf{U}_3 \boldsymbol{\Sigma}_3 \mathbf{V}_3^3.\end{aligned}\tag{45}$$

Let $\mathbf{U}_4 = \mathbf{U}_2(:, 1 : N_{s1}) \in \mathbb{C}^{N_b \times N_{s1}}$ denotes the first N_{s1} columns of \mathbf{U}_2 , $\mathbf{U}_5 = \mathbf{U}_3(:, 1 : N_{s2}) \in \mathbb{C}^{N_b \times N_{s2}}$ denotes the first N_{s2} columns of \mathbf{U}_3 , and $\mathbf{U}_{q,k} = [\mathbf{U}_4, \mathbf{U}_5] \in \mathbb{C}^{N_b \times N_s}$. Then, the transmit covariance matrix \mathbf{Q}_k is given by (with a slight abuse of notations)

$$\mathbf{Q}_k = \mathbf{U}_{q,k} \boldsymbol{\Lambda}_{q,k} \mathbf{U}_{q,k}^H,\tag{46}$$

where $\boldsymbol{\Lambda}_{q,k} = \text{diag}(q_{k,1}, q_{k,2}, \dots, q_{k,N_s})$ and $q_{k,i}$ represents the amount of power allocated to the i -th data stream.

The result in (44) is only for one subcarrier. Then, considering all of the subcarriers, the ergodic capacity can be approximated by

$$\begin{aligned}C_{app} &= \mathbb{E}_{\alpha_{g,i}, \alpha_{t,i}} \left[\frac{1}{K + N_{cp}} \sum_{k=1}^K \sum_{i=1}^{N_{s1}} \log_2 \left(1 + \frac{P_T N_b N_u N_r^2}{\sigma^2 L_g L_t} q_{k,i} d_{ut,k,i} d_{bg,k,i} d_{r,k,i} |\alpha_{g,i}|^2 |\alpha_{t,i}|^2 \right) \right] \\ &+ \mathbb{E}_{\alpha_{h,i}} \left[\frac{1}{K + N_{cp}} \sum_{k=1}^K \sum_{i=1}^{N_{s2}} \log_2 \left(1 + \frac{P_T N_b N_u}{\sigma^2 L_h} q_{k,N_{s1}+i} d_{uh,k,i} d_{bh,k,i} |\alpha_{h,i}|^2 \right) \right].\end{aligned}\tag{47}$$

B. Proof of Theorem 2

When the transmit covariance matrix \mathbf{Q}_k is adopted as (46) and SNR goes to infinity, we have

$$\begin{aligned}C_h &= \mathbb{E}_{\mathbf{H}_{\text{eff},k}} \left[\frac{1}{K + N_{cp}} \sum_{k=1}^K \sum_{i=1}^{N_s} \log_2 \left(\frac{P_T}{\sigma^2} q_{i,k} \lambda_i (\mathbf{T}_k \boldsymbol{\Theta} \mathbf{G}_k \mathbf{G}_k^H \boldsymbol{\Theta}^H \mathbf{T}_k^H + \mathbf{H}_k \mathbf{H}_k^H) \right) \right] \\ &= \mathbb{E}_{\mathbf{H}_{\text{eff},k}} \left[\frac{1}{K + N_{cp}} \sum_{k=1}^K \sum_{i=1}^{N_{s1}} \log_2 \left(\frac{P_T}{\sigma^2} q_{i,k} \lambda_i (\mathbf{T}_k \boldsymbol{\Theta} \mathbf{G}_k \mathbf{G}_k^H \boldsymbol{\Theta}^H \mathbf{T}_k^H) \right) \right] \\ &+ \mathbb{E}_{\mathbf{H}_{\text{eff},k}} \left[\frac{1}{K + N_{cp}} \sum_{k=1}^K \sum_{i=1}^{N_{s2}} \log_2 \left(\frac{P_T}{\sigma^2} q_{N_{s1}+i,k} \lambda_i (\mathbf{H}_k \mathbf{H}_k^H) \right) \right].\end{aligned}\tag{48}$$

Using the results in [22, Proposition 2] and [29, Theorem 3], we have

$$\begin{aligned}C_h^{upper} &= \sum_{k=1}^K \sum_{i=1}^{N_{s1}} \frac{1}{(K + N_{cp}) \ln 2} \left(2\psi(1) + \ln \left(\frac{P_T N_b N_u N_r^2 \sigma_g^2 \sigma_t^2}{\sigma^2 L_g L_t} q_{k,i} d_{ut,k,i} d_{bg,k,i} d_{r,k,i} \right) \right) \\ &+ \sum_{k=1}^K \sum_{i=1}^{N_{s2}} \frac{1}{(K + N_{cp}) \ln 2} \left(\psi(1) + \ln \left(\frac{P_T N_b N_u \sigma_h^2}{\sigma^2 L_h} q_{k,N_{s1}+i} d_{uh,k,i} d_{bh,k,i} \right) \right),\end{aligned}\tag{49}$$

where $\psi(x) = \frac{d}{dx} \ln \Gamma(x)$ is the Digamma function and $\psi(1) = -\gamma$.

C. Proof of Theorem 3

Applying Jensen's inequality $\mathbb{E}\{\log_2(1+x)\} \leq \log_2(1+\mathbb{E}\{x\})$ for $x \geq 0$ to (17), we have

$$\begin{aligned}
C_{app} &= \mathbb{E}_{\alpha_{g,i}, \alpha_{t,i}} \left[\frac{1}{K+N_{cp}} \sum_{k=1}^K \sum_{i=1}^{N_{s1}} \log_2 \left(1 + \frac{P_T N_b N_u N_r^2}{\sigma^2 L_g L_t} q_{k,i} d_{ut,k,i} d_{bg,k,i} d_{r,k,i} |\alpha_{g,i}|^2 |\alpha_{t,i}|^2 \right) \right] \\
&\quad + \mathbb{E}_{\alpha_{h,i}} \left[\frac{1}{K+N_{cp}} \sum_{k=1}^K \sum_{i=1}^{N_{s2}} \log_2 \left(1 + \frac{P_T N_b N_u}{\sigma^2 L_h} q_{k,N_{s1}+i} d_{uh,k,i} d_{bh,k,i} |\alpha_{h,i}|^2 \right) \right] \\
&\leq \frac{1}{K+N_{cp}} \sum_{k=1}^K \sum_{i=1}^{N_{s1}} \log_2 \left(1 + \frac{P_T N_b N_u N_r^2}{\sigma^2 L_g L_t} q_{k,i} d_{ut,k,i} d_{bg,k,i} d_{r,k,i} \mathbb{E}(|\alpha_{g,i}|^2 |\alpha_{t,i}|^2) \right) \\
&\quad + \frac{1}{K+N_{cp}} \sum_{k=1}^K \sum_{i=1}^{N_{s2}} \log_2 \left(1 + \frac{P_T N_b N_u}{\sigma^2 L_h} q_{k,N_{s1}+i} d_{uh,k,i} d_{bh,k,i} \mathbb{E}(|\alpha_{h,i}|^2) \right) \\
&\stackrel{(a)}{=} \frac{1}{K+N_{cp}} \sum_{k=1}^K \sum_{i=1}^{N_{s1}} \log_2 \left(1 + \frac{P_T N_b N_u N_r^2 \sigma_{g,i}^2 \sigma_{t,i}^2}{\sigma^2 L_g L_t} q_{k,i} d_{ut,k,i} d_{bg,k,i} d_{r,k,i} \right) \\
&\quad + \frac{1}{K+N_{cp}} \sum_{k=1}^K \sum_{i=1}^{N_{s2}} \log_2 \left(1 + \frac{P_T N_b N_u \sigma_{h,i}^2}{\sigma^2 L_h} q_{k,N_{s1}+i} d_{uh,k,i} d_{bh,k,i} \right) \\
&\triangleq C_{Jen1},
\end{aligned} \tag{50}$$

where (a) holds due to the following fact. $\alpha_{g,i} \sim \mathcal{CN}(0, \sigma_{g,i}^2)$, $\alpha_{t,i} \sim \mathcal{CN}(0, \sigma_{t,i}^2)$, and $\alpha_{g,i}$ and $\alpha_{t,i}$ are independent with each other. Then, $|\alpha_{g,i}|^2 \sim \exp(\frac{1}{\sigma_{g,i}^2})$, $|\alpha_{t,i}|^2 \sim \exp(\frac{1}{\sigma_{t,i}^2})$, and $\mathbb{E}(|\alpha_{g,i}|^2 |\alpha_{t,i}|^2) = \sigma_{g,i}^2 \sigma_{t,i}^2$. Similarly, $\mathbb{E}(|\alpha_{h,i}|^2) = \sigma_{h,i}^2$.

D. Proof of Proposition 2

When $\mathbf{Q}_k = \frac{1}{KN_b} \mathbf{I}_{N_b}$, we have

$$\begin{aligned}
C_k &= \mathbb{E}_{\mathbf{H}_{\text{eff},k}} \left[\log_2 \det \left(\mathbf{I}_{N_u} + \frac{P_T}{\sigma^2} \mathbf{H}_{\text{eff},k} \mathbf{Q}_k \mathbf{H}_{\text{eff},k}^H \right) \right] \\
&= \mathbb{E}_{\mathbf{H}_{\text{eff},k}} \left[\log_2 \det \left(\mathbf{I}_{N_u} + \frac{P_T}{\sigma^2 KN_b} \mathbf{H}_{\text{eff},k} \mathbf{H}_{\text{eff},k}^H \right) \right] \\
&= \mathbb{E}_{\mathbf{H}_{\text{eff},k}} \left[\sum_{i=1}^{N_s} \log_2 \left(1 + \frac{P_T}{\sigma^2 KN_b} \lambda_i(\mathbf{H}_{\text{eff},k} \mathbf{H}_{\text{eff},k}^H) \right) \right].
\end{aligned} \tag{51}$$

The following derivations are similar to Appendix A. Thus, it is omitted here.

REFERENCES

- [1] A. Ghosh, T. A. Thomas, M. C. Cudak, R. Ratasuk, P. Moorut, F. W. Vook, T. S. Rappaport, G. R. MacCartney, S. Sun, and S. Nie, "Millimeter-wave enhanced local area systems: A high-data-rate approach for future wireless networks," *IEEE J. Sel. Areas Commun.*, vol. 32, no. 6, pp. 1152–1163, Jun. 2014.
- [2] R. W. Heath, N. Gonzalez-Prelcic, S. Rangan, W. Roh, and A. M. Sayeed, "An overview of signal processing techniques for millimeter wave MIMO systems," *IEEE J. Sel. Topics Signal Process.*, vol. 10, no. 3, pp. 436–453, Apr. 2016.
- [3] Q. Wu and R. Zhang, "Towards smart and reconfigurable environment: Intelligent reflecting surface aided wireless network," *IEEE Commun. Mag.*, vol. 58, no. 1, pp. 106–112, Jan. 2020.
- [4] S. Gong, X. Lu, D. T. Hoang, D. Niyato, L. Shu, D. I. Kim, and Y.-C. Liang, "Toward smart wireless communications via intelligent reflecting surfaces: A contemporary survey," *IEEE Commun. Surv. Tutor.*, vol. 22, no. 4, pp. 2283–2314, Jun. 2020.
- [5] R. Alghamdi, R. Alhadrami, D. Alhothali, H. Almorad, A. Faisal, S. Helal, R. Shalabi, R. Asfour, N. Hammad, A. Shams, N. Saeed, H. Dahrouj, T. Y. Al-Naffouri, and M.-S. Alouini, "Intelligent surfaces for 6G wireless networks: A survey of optimization and performance analysis techniques," *IEEE Access*, vol. 8, pp. 202 795–202 818, Oct. 2020.
- [6] Q. Wu and R. Zhang, "Intelligent reflecting surface enhanced wireless network via joint active and passive beamforming," *IEEE Trans. Wireless Commun.*, vol. 18, no. 11, pp. 5394–5409, Nov. 2019.
- [7] H. Guo, Y.-C. Liang, J. Chen, and E. G. Larsson, "Weighted sum-rate maximization for reconfigurable intelligent surface aided wireless networks," *IEEE Trans. Wireless Commun.*, vol. 19, no. 5, pp. 3064–3076, May 2020.
- [8] S. Zhang and R. Zhang, "Capacity characterization for intelligent reflecting surface aided MIMO communication," *IEEE J. Sel. Areas Commun.*, vol. 38, no. 8, pp. 1823–1838, Aug. 2020.
- [9] P. Wang, J. Fang, L. Dai, and H. Li, "Joint transceiver and large intelligent surface design for massive MIMO mmwave systems," *IEEE Trans. Wireless Commun.*, vol. 20, no. 2, pp. 1052–1064, Feb. 2021.
- [10] B. Wang, F. Gao, S. Jin, H. Lin, and G. Y. Li, "Spatial- and frequency-wideband effects in millimeter-wave massive MIMO systems," *IEEE Trans. Signal Process.*, vol. 66, no. 13, pp. 3393–3406, Jul. 2018.
- [11] B. Ning, Z. Tian, Z. Chen, C. Han, J. Yuan, and S. Li, "Prospective beamforming technologies for ultra-massive MIMO in terahertz communications: A tutorial," 2021. [Online]. Available: <https://arxiv.org/abs/2107.03032>
- [12] Y. Yang, B. Zheng, S. Zhang, and R. Zhang, "Intelligent reflecting surface meets OFDM: Protocol design and rate maximization," *IEEE Trans. Commun.*, vol. 68, no. 7, pp. 4522–4535, Jul. 2020.
- [13] Y. Yang, S. Zhang, and R. Zhang, "Irs-enhanced OFDMA: Joint resource allocation and passive beamforming optimization," *IEEE Wireless Commun. Lett.*, vol. 9, no. 6, pp. 760–764, Jun. 2020.
- [14] Y. Chen, D. Chen, and T. Jiang, "Beam-squint mitigating in reconfigurable intelligent surface aided wideband mmwave communications," in *Proc. IEEE WCNC*, Apr. 2021, pp. 1–6.
- [15] H. Li, R. Liu, M. Liy, Q. Liu, and X. Li, "IRS-enhanced wideband MU-MISO-OFDM communication systems," in *Proc. IEEE WCNC*, May 2020, pp. 1–6.
- [16] P. Nuti, E. Balti, and B. L. Evans, "Spectral efficiency optimization for mmwave wideband MIMO RIS-assisted communication," 2021. [Online]. Available: <https://arxiv.org/abs/2201.01739>
- [17] K. Ying, Z. Gao, S. Lyu, Y. Wu, H. Wang, and M.-S. Alouini, "GMD-based hybrid beamforming for large reconfigurable intelligent surface assisted millimeter-wave massive MIMO," *IEEE Access*, vol. 8, pp. 19 530–19 539, Jan. 2020.
- [18] S. H. Hong, J. Park, S.-J. Kim, and J. Choi, "Hybrid beamforming for intelligent reflecting surface aided millimeter wave MIMO systems," 2022. [Online]. Available: <https://arxiv.org/abs/2105.13647>

- [19] Z. Zhang and L. Dai, "A joint precoding framework for wideband reconfigurable intelligent surface-aided cell-free network," *IEEE Trans. Signal Process.*, vol. 69, pp. 4085–4101, Jun. 2021.
- [20] W. Jiang, B. Chen, S. Garg, J. Nie, J. Zhao, and Z. Xiong, "Joint transmit precoding and reflect beamforming for IRS-assisted MIMO-OFDM secure communications," in *Proc. IEEE GLOBECOM*, Dec. 2021, pp. 1–6.
- [21] W. Jiang, B. Chen, J. Zhao, Z. Xiong, and Z. Ding, "Joint active and passive beamforming design for the IRS-assisted MIMOME-OFDM secure communications," *IEEE Trans. Veh. Technol.*, vol. 70, no. 10, pp. 10 369–10 381, Oct. 2021.
- [22] R. Li, S. Sun, Y. Chen, C. Han, and M. Tao, "RIS-assisted millimeter-wave MIMO communication systems: Ergodic capacity analysis and optimization," 2022. [Online]. Available: <https://arxiv.org/abs/2202.06564>
- [23] X. Yu, J.-C. Shen, J. Zhang, and K. B. Letaief, "Alternating minimization algorithms for hybrid precoding in millimeter wave MIMO systems," *IEEE J. Sel. Topics Signal Process.*, vol. 10, no. 3, pp. 485–500, Apr. 2016.
- [24] Y. Chen, D. Chen, T. Jiang, and L. Hanzo, "Channel-covariance and angle-of-departure aided hybrid precoding for wideband multiuser millimeter wave MIMO systems," *IEEE Trans. Commun.*, vol. 67, no. 12, pp. 8315–8328, Dec. 2019.
- [25] M. Wang, F. Gao, S. Jin, and H. Lin, "An overview of enhanced massive MIMO with array signal processing techniques," *IEEE J. Sel. Topics Signal Process.*, vol. 13, no. 5, pp. 886–901, Sep. 2019.
- [26] A. Alkhateeb, O. El Ayach, G. Leus, and R. W. Heath, "Channel estimation and hybrid precoding for millimeter wave cellular systems," *IEEE J. Sel. Topics Signal Process.*, vol. 8, no. 5, pp. 831–846, Oct. 2014.
- [27] A. W. Marshall, I. Olkin, and B. C. Arnold, *Inequalities: theory of majorization and its applications*. Springer, 1979, vol. 143.
- [28] J. Chen, "When does asymptotic orthogonality exist for very large arrays?" in *Proc. IEEE GLOBECOM*, Dec. 2013, pp. 4146–4150.
- [29] X. Yang, X. Li, S. Zhang, and S. Jin, "On the ergodic capacity of mmwave systems under finite-dimensional channels," *IEEE Trans. Wireless Commun.*, vol. 18, no. 11, pp. 5440–5453, Nov. 2019.
- [30] H. N. Nagaraja, "Order statistics from independent exponential random variables and the sum of the top order statistics," in *Advances in Distribution Theory, Order Statistics, and Inference*. Springer, 2006, pp. 173–185.
- [31] A. Tulino, A. Lozano, and S. Verdu, "Capacity-achieving input covariance for single-user multi-antenna channels," *IEEE Trans. Wireless Commun.*, vol. 5, no. 3, pp. 662–671, Mar. 2006.
- [32] P. Almers, F. Tufvesson, O. Edfors, and A. Molisch, "Measured capacity gain using water filling in frequency selective MIMO channels," in *IEEE Int. Symp. Personal, Indoor and Mobile Radio Commun.*, vol. 3, 2002, pp. 1347–1351 vol.3.
- [33] P.-A. Absil, R. Mahony, and R. Sepulchre, *Optimization Algorithms on Matrix Manifolds*. Princeton University Press, 2009. [Online]. Available: <https://doi.org/10.1515/9781400830244>
- [34] M. K. Samimi and T. S. Rappaport, "3-D millimeter-wave statistical channel model for 5G wireless system design," *IEEE Trans. Microw. Theory Techn.*, vol. 64, no. 7, pp. 2207–2225, Jul. 2016.